INTERNATIONAL JOURNAL FOR NUMERICAL METHODS IN FLUIDS
Int. J. Numer. Meth. Fluids 2007; **55**:985–1018
Published online 24 April 2007 in Wiley InterScience (www.interscience.wiley.com). DOI: 10.1002/fld.1503

Direct simulation of two-dimensional turbulent flow over a surface-mounted obstacle

V. P. Fragos[1], S. P. Psychoudaki[1] and N. A. Malamataris[2,*,†]

[1]*Department of Hydraulics, Soil Sciences and Agricultural Engineering, Aristotle University of Thessaloniki, GR-54124 Thessaloniki, Greece*
[2]*Department of Mechanical Engineering, Technological and Educational Institute of W. Macedonia, GR-50100 Kila, Greece*

SUMMARY

Two-dimensional turbulent flow over a surface-mounted obstacle is studied as a numerical experiment that takes place in a wind tunnel. The transient Navier–Stokes equations are solved directly with Galerkin finite elements. The Reynolds number defined with respect to the height of the wind tunnel is 12 518. Instantaneous streamline patterns are shown that give a complete picture of the flow phenomena. Energy and enstrophy spectra yield the dual cascade of two-dimensional turbulence and the -1 power law decay of enstrophy. Mean values of velocities and root mean square fluctuations are compared with the available experimental results. Other statistical characteristics of turbulence such as Eulerian autocorrelation coefficients, longitudinal and lateral coefficients are also computed. Finally, oscillation diagrams of computed velocity fluctuations yield the chaotic behaviour of turbulence. Copyright © 2007 John Wiley & Sons, Ltd.

Received 30 October 2006; Revised 3 March 2007; Accepted 11 March 2007

KEY WORDS: two-dimensional turbulence; energy and enstrophy spectra; calculation of autocorrelation and cross-correlation functions; Galerkin finite elements; chaos

1. INTRODUCTION

Turbulent flow over a surface-mounted obstacle is a fundamental problem in fluid mechanics having a wide range of applications in all domains of engineering science, as recently reviewed by Fragos *et al.* [1], Larichkin and Yakovenko [2], Lohász *et al.* [3]. Although the flow has received a lot of attention from the engineering community, it is still an open-ended problem partly due to its complicated geometry and partly due to the unresolved issues of turbulence.

*Correspondence to: N. A. Malamataris, Department of Mechanical Engineering, Technological and Educational Institute of W. Macedonia, GR-50100 Kila, Greece.
†E-mail: nikolaos_malamataris@yahoo.gr, nikolaos@eng.auth.gr

Contract/grant sponsor: Office of the Hellenic Foundation for Research

The term surface-mounted obstacle is also ambigously used in the literature. By this term, some authors mean a cubic or a prismatically shaped obstacle, where the fluid flows over the top and around the sides. This is clearly a three-dimensional flow that takes place in the three-dimensional space. A recent solution to this problem using adaptive stabilized Galerkin finite elements with duality has been given by Hoffman and Johnson [4]. Other authors examine the flow over a cubic or a prismatically shaped obstacle having a width that extends up to the walls of a wind tunnel, where the obstacle is placed. This case is a two-dimensional flow, that takes place in the two-dimensional space, where any three-dimensional effect is generated from the existence of walls or from turbulence. This flow situation is the subject of this work.

For this particular flow, there is some recent experimental work in the turbulent regime conducted by Acharya *et al.* [5] and Larichkin and Yakovenko [2] for obstacles with rectangular cross-section of aspect ratio 1:1. There are also attempts to study this flow computationally by Acharya *et al.* [5], Hwang *et al.* [6] who used k–ε models with a finite difference method and Lohász *et al.* [3] who approached the problem with large eddy simulation and a finite volume method. In this work, the two-dimensional flow over a surface-mounted obstacle is studied computationally solving the unsteady Navier–Stokes equations in primitive variable formulation with standard Galerkin finite elements. The experimental set-up and the process parameters of the study of Acharya *et al.* [5] are taken for comparison with the numerical results of this work.

Very recently, John and Liakos [7] studied the flow over a surface-mounted obstacle in the laminar flow regime. They solved the transient Navier–Stokes equations directly focusing on the evolution of the reattachment points of the recirculating vortices, which develop downstream of the obstacle as a function of the slip coefficient. Psychoudaki *et al.* [8] made a complete study of this flow using the same parameters as in the present work focusing on the first stages of its development. They calculated the positions of separation and reattachment of vortices, the value of shear stress and the growth of the boundary layer from the initiation of the flow up to the inception of turbulence.

Unlike other approaches in computational fluid mechanics, the finite element code of this work has been verified by Fragos *et al.* [1] in the laminar flow regime with available experimental data. The results of that study have been used by John [9] and Oden and Prudhomme [10] for the evaluation of their numerical schemes. The ability of the code to correctly predict this flow at moderate Reynolds numbers (order of 100) led the authors to use the following strategy in the study of two-dimensional turbulence: direct computation of turbulent flow may be simply viewed as the execution of an available laminar flow code at a higher Reynolds number by adding the time derivative to the governing equations.

So far, two-dimensional turbulent flows have been primarily computed for bounded flows using the streamline vorticity formulation of the Navier–Stokes equations, as discussed in many reviews including Kraichnan [11] and Nazarenko and Laval [12]. The primary interest of these works was to predict the inverse energy cascade and the forward enstrophy cascade, which have been studied theoretically by Batchelor [13] and Kraichnan [11], who extended the work of Kolmogoroff in two dimensions.

In the direct numerical simulation of three-dimensional flows, the Navier–Stokes equations are solved in primitive variable formulation. As thoroughly discussed in many reviews of this subject including Friedrich *et al.* [14], Moin and Mahesh [15] and Hunt *et al.* [16], all aspects of turbulence may be studied with this method like cross-correlations, energy spectra, instantaneous *versus* mean features of the flow along with computational issues like proper choice of initial conditions, inflow and outflow boundary conditions.

DOI: 10.1002/fld

In this work, the issues of both two-dimensional turbulence and direct numerical simulation of turbulent flows are addressed in the study of two-dimensional turbulent flow over a surface-mounted obstacle with square cross-section.

In the following, the governing equations are presented along with the computational domain and the parameters of the flow. The issues of initial condition and inflow as well as outflow boundary condition are examined next, followed by the finite element formulation and the computational details. The results of this work are subsequently discussed and finally conclusions are drawn.

2. GOVERNING EQUATIONS AND FLOW PARAMETERS

The computational domain for the turbulent flow over a surface-mounted obstacle is shown in Figure 1. A Newtonian fluid of constant viscosity and density approaches with uniform u-velocity a wind tunnel of rectangular cross-section. At the entrance of the tunnel, the fluid is decelerated along the wall due to the no-slip boundary condition. The fluid continues its motion through the tunnel and hits the surface-mounted obstacle, which has a square cross-section. The flow separates forming recirculation zones both upstream and downstream of the obstacle. The fluid leaves the computational domain after a certain distance downstream.

For a two-dimensional isothermal turbulent flow of an incompressible Newtonian fluid, the dimensionless Navier–Stokes equations are:

$$\nabla \cdot \mathbf{u} = 0 \tag{1}$$

$$\frac{\partial \mathbf{u}}{\partial t} + \mathbf{u} \cdot \nabla \mathbf{u} = -\nabla p + \frac{1}{Re} \nabla \{\nabla \mathbf{u} + (\nabla \mathbf{u})^{\mathrm{T}}\} \tag{2}$$

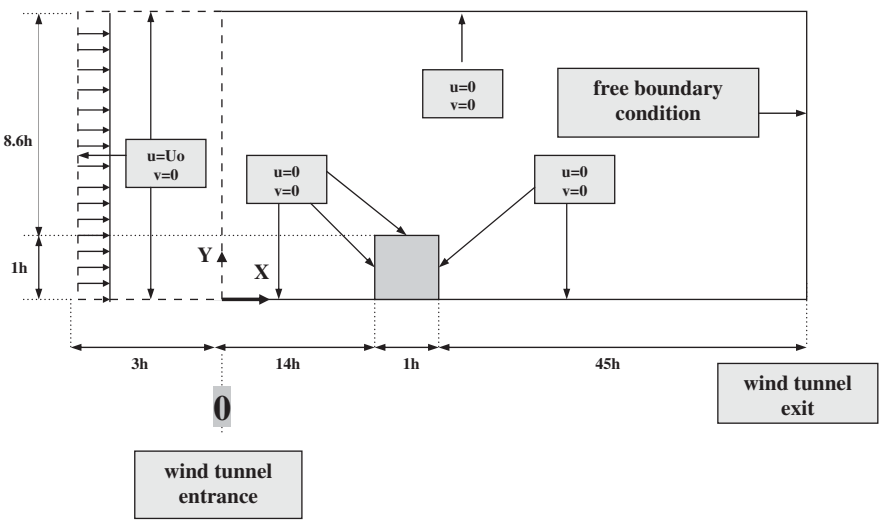

Figure 1. Computational domain of the two-dimensional turbulent flow over a surface-mounted obstacle with a square cross-section, placed in a wind tunnel.

DOI: 10.1002/fld

The governing equations are given here in their primitive variable formulation. For two-dimensional turbulence, it is more common to use the streamline vorticity formulation. For this flow, though, this formulation is not suitable, due to the singularity at the corners of the obstacle. The magnitude of vorticity goes to infinity there, as shear stress is infinite [17], which causes divergence of any discretization scheme to be applied.

Equations (1) and (2) represent conservation of mass and momentum, respectively. Equation (2) is written in its stress divergence form [18, p. 362]. This choice is better suited for finite elements, because it leads to weak formulations in a more straightforward way than its simpler Lagrangian form.

The governing equations have been rendered dimensionless, by choosing the uniform approaching velocity of the fluid U_0 as the characteristic velocity and the height of the obstacle h as the characteristic length. The reference time t_r is then the ratio h/U_0. In the governing equations, $\mathbf{u} = (u, v)$ is the velocity vector of the fluid with u and v its components in the x and y direction, respectively, t is the time, p is the pressure and $Re = U_0 h/\nu$ is the Reynolds number with respect to the height of the obstacle, with ν the kinematic viscosity of the fluid. The pressure p has been non-dimensionalized with term ρU_0^2, with ρ being the density of the fluid. The time t has been non-dimensionalized with reference time t_r.

The dimensions of the computational domain and the Reynolds number were chosen to match the parameters of the laboratory experiment conducted by Acharya *et al.* [5]. In keeping with their conditions, the height of the obstacle is $h = 6.35$ mm, the height of the tunnel is $H = 9.6h$ and the approaching velocity of the fluid is $U_0 = 3.225$ m/s. Air was chosen as a working fluid with a kinematic viscosity $\nu = 1.57 \cdot 10^{-5}$ m^2/s and a density $\rho = 1.2$ kg/m^3. These values of the process parameters yield a Reynolds number of 1304. It should be noted that the flow is in the fully turbulent regime, because the Reynolds number is 12 518 if it is computed using the height of the tunnel H as a characteristic length. All the other dimensions of the computational domain are depicted in Figure 1 as functions of the height of the obstacle h.

In order to solve the problem, appropriate boundary and initial conditions must be chosen, which are discussed in the next section.

3. BOUNDARY AND INITIAL CONDITIONS

The boundary conditions for this flow are depicted in Figure 1 and given in the equations below:

at the entrance:

$$u = U_0 \tag{3}$$

$$v = 0 \tag{4}$$

top and bottom boundaries, *upstream the wind tunnel*:

$$u = U_0 \tag{5}$$

$$v = 0 \tag{6}$$

top and bottom walls of the wind tunnel:

$$u = 0 \tag{7}$$

$$v = 0 \tag{8}$$

DOI: 10.1002/fld

along the walls of obstacle:

$$u = 0 \tag{9}$$

$$v = 0 \tag{10}$$

at the outflow: *free boundary condition*

Equations (3) and (4) impose a uniform undisturbed velocity profile that defines the flow rate entering the wind tunnel. By choosing this boundary condition at the inlet, we avoid the introduction of any turbulent fluctuations numerically. In this way, the numerical experiment resembles the actual laboratory experiment regarding the initiation of turbulence, where the inlet velocity profile upstream of the wind tunnel is free of any disturbance, as it enters the test section. In this study, the only source of turbulence is the disturbance of the fluid flow due to the presence of the obstacle.

This set-up of inlet boundary conditions is widely used in transient direct numerical simulations of laminar flows [18, 19]. However, this concept is usually combined with white noise or inflow fluctuations when the flow is turbulent, in order to initiate turbulence in the calculation. In this work, we avoid any artificial initiation of turbulence by numerical means, which is also going to be pointed out in the discussion of initial conditions that follows. Hoffman and Johnson [4, p. 10] also used this strategy (Equations (3) and (4)) in the flow past a square cylinder.

Equations (5) and (6) are tow tank boundary conditions. Equations (7)–(10) are no-slip boundary conditions along the solid walls of the computational domain.

Special care must be taken at the outflow of the domain for turbulent flows, as thoroughly discussed by Friedrich *et al.* [14], Moin and Mahesh [15] and Le *et al.* [20], due to the fact that vortical structures that are generated must travel downstream and leave the computational domain without any disturbance of the interior flow. This demand for suitable outflow boundary conditions extends to other flow situations as well like compressible flows, as reviewed by Colonius [21], or laminar flows in unbounded domains, as discussed by Malamataris [22], Malamataris and Panastasiou [23], Panastasiou *et al*. [24], Sani and Gresho [25]. In general, the issue of the proper boundary condition at the outflow of a computational domain is an open-ended problem for any type of flow, since the magnitudes of the dependent variables are unknown *a priori*.

Common practice in the direct numerical simulation community is the use of convective boundary conditions at the outflow. This is in accordance with a Sommerfeld-type radiation boundary condition that has already been used by Orlanski [26] in computations of atmospheric flows, where the computational domain is by definition unbounded. A different approach has been chosen by Malamataris [22] and Malamataris and Panastasiou [23] who used the free boundary condition, in order to solve laminar free surface flows with convective waves that pass through the artificial outflow. In the work of Papanastasiou *et al.* [24], it has also been shown that this boundary condition performs well in separated flows, where the recirculation region is cut at the outflow.

One may arrive at a similar condition called transparent outflow boundary condition by using a special Galerkin finite element method based on a variational formulation of the Navier–Stokes, as discussed by Ranacher [19, p. 12]. The transparent outflow boundary condition has been successfully used by Hoffman and Johnson [4] in their study of three-dimensional turbulent flows using adaptive stabilized Galerkin finite elements.

The concept of the free boundary condition is used for this flow problem at the outflow of the computational domain (see Figure 1). However, it is beyond the scope of this work to go into the details of the implementation of this idea or into its mathematical insight, which has been accomplished by Sani and Gresho [25], Heinrich and Vionnet [27], Griffiths [28] and Renardy [29].

DOI: 10.1002/fld

Zienkiewicz and Taylor [30, vol. 3, p. 81] also suggest its use in their discussion about outflow boundary conditions in unbounded flows. It is impossible to express the free boundary condition analytically at this step, as is the case with traditional essential or natural boundary conditions, because this concept is derived from the weak form of the weighted Navier–Stokes residuals. First, the finite element method must be presented, in order to briefly outline its inclusion in the final formulation of the equations to be solved and this is done in the next section.

Another major issue in the direct numerical simulation of turbulence is the choice of the proper initial condition, due to the high value of the Reynolds number. This issue is of general interest to the community of computational fluid mechanics, like the case of outflow boundary conditions, because convergence may be impossible if the initial guess is far from the solution, even at steady-state problems of laminar flows with moderate Reynolds number (order of 100). However, the computational cost is low for steady-state problems and convergence to the desired Reynolds number is achieved with the incremental Reynolds number solution: a solution with a lower Reynolds number is used as a first guess to a higher value of Reynolds and so on until the final solution.

This method is impossible in the direct simulation of turbulent flow. It is common practice to generate random fluctuations superimposed on a computed or measured mean velocity field and let the flow go until it reaches its final turbulent state, as discussed by Friedrich *et al.* [14]. In addition, this practice is enhanced either by imposing an inlet velocity profile in accordance with experimental data [4, p. 12] or by using instantaneous results of large eddy simulation of channel flow [31, p. 927]. Although this procedure is effective and computationally economical, it has the disadvantage of introducing artificial physics in the computation. Even if turbulent flows get independent of their initial conditions, there is a lack of elegance in this method.

A different approach has been taken in this work. The steady-state solution of laminar flow at $Re = 1$ was chosen as the initial condition. This numerical solution has been validated with laboratory experimental data, in the work by Fragos *et al.* [1]. The streamlines for this flow are shown in Figure 2. By executing the computer program, the flow develops from its initial laminar state to fully developed turbulence. Hence, this approach has the advantage that the transition from laminar to turbulent flow is also computed in addition to the study of turbulence, as is shown

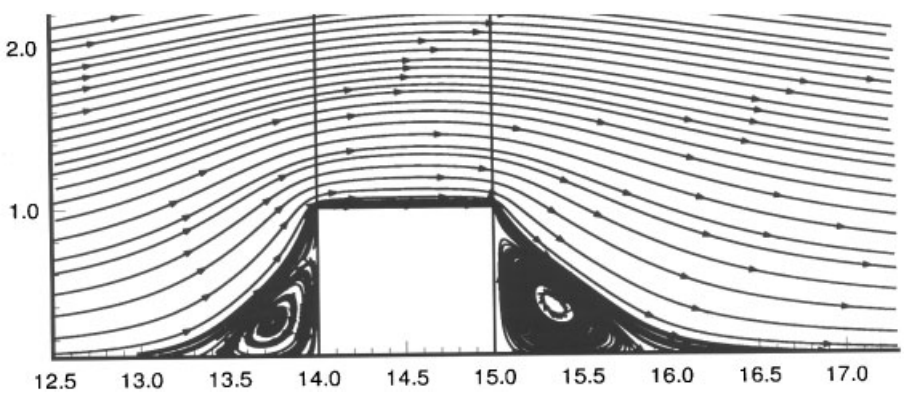

Figure 2. Streamlines of the laminar flow over a surface-mounted obstacle at Reynolds number 1 with respect to the obstacle height, chosen as the initial condition for this work. Details of the solution for this flow are given in the work of Fragos *et al.* [1].

DOI: 10.1002/fld

in Figures 4–7. In this way, the numerical experiment is in accordance with the experience of experimentalists who study flow phenomena at high Reynolds numbers by gradually adjusting the flow rate to the desired level. Additionally, any artificialities introduced numerically are avoided. In this way, the numerical experiment is closer to the real world. After all, turbulence may originate from instabilities of laminar flows, as discussed by Hunt *et al.* [16].

4. FINITE ELEMENT FORMULATION AND COMPUTATIONAL DETAILS

The computational mesh used in this work is shown in Figure 3. It consists of rectangular finite elements of different sizes with nine nodes in each of them. Standard Galerkin finite elements [18, 30, 32] are used in this work to solve the governing equations along with the appropriate initial and boundary conditions. Velocities and pressure are approximated with quadratic ϕ^i and linear ψ^i basis functions in each element as:

$$u = \sum_{i=1}^{9} u_i \phi^i, \quad v = \sum_{i=1}^{9} v_i \phi^i, \quad p = \sum_{i=1}^{4} p_i \psi^i$$

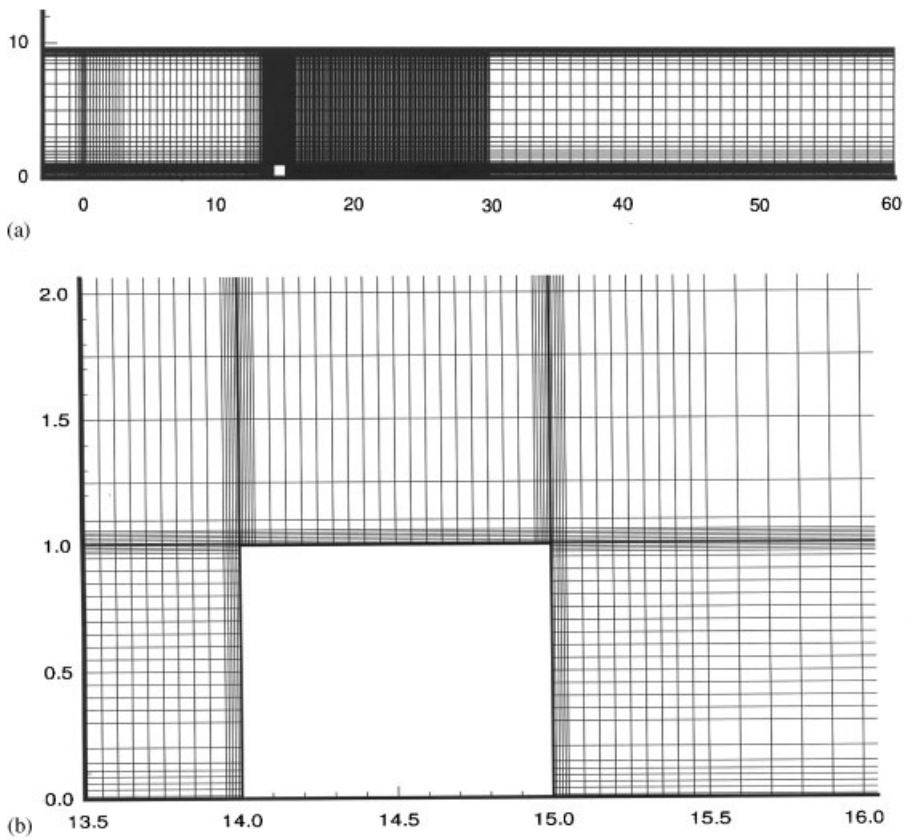

Figure 3. (a) Computational mesh used in this work and (b) details of mesh tessellation around the obstacle.

DOI: 10.1002/fld

These approximations are inserted into Equations (1) and (2), which are weighted integrally with basis functions ψ^i and ϕ^i, respectively, in order to obtain the following continuity, R^i_{C}, and momentum, R^i_{M}, residuals:

$$R^i_{\mathrm{C}} = \int_V \nabla \cdot \mathbf{u}\psi^i \, \mathrm{d}V \tag{11}$$

$$R^i_{\mathrm{M}} = \int_V \left[\frac{\partial \mathbf{u}}{\partial t} + \mathbf{u} \cdot \nabla \mathbf{u} - \nabla \cdot \left(-p\mathbf{I} + \frac{1}{Re}\{\nabla \mathbf{u} + (\nabla \mathbf{u})^{\mathrm{T}}\} \right) \right] \phi^i \, \mathrm{d}V \tag{12}$$

By applying the divergence theorem, in order to decrease the order of differentiation and project possible natural (Neumann type) boundary conditions, Equation (12) reduces to:

$$R^i_{\mathrm{M}} = \int_V \left[\left(\frac{\partial \mathbf{u}}{\partial t} + \mathbf{u} \cdot \nabla \mathbf{u} \right) \phi^i + \left(-p\mathbf{I} + \frac{1}{Re}\{\nabla \mathbf{u} + (\nabla \mathbf{u})^{\mathrm{T}}\} \right) \cdot \nabla \phi^i \right] \mathrm{d}V$$

$$- \int_S \mathbf{n} \cdot \left[-p\,\mathbf{I} + \frac{1}{Re}\{\nabla \mathbf{u} + (\nabla \mathbf{u})^{\mathrm{T}}\} \right] \phi^i \, \mathrm{d}S \tag{13}$$

Since essential (Dirichlet type) boundary conditions for u and v are applied to all boundaries of the domain except for the outflow, Equation (13) is going to be replaced by Equations (3)–(10). The integral over the volume of Equation (13) along with Equation (11) are evaluated at all the interior nodes of the computational domain. At the exit of the domain, the surface integral of Equation (13) is added to all exit nodes, which is the application of the free boundary condition [22, 24].

In this way, the solution of the outflow is given by the governing equations without imposing any arbitrary boundary condition, which distorts the physics of the flow there and may propagate into the interior of the domain. In order to examine the error that is introduced in the code at the outflow, it is common practice to run the computer code at domains with shorter lengths and check how velocity and pressure fields change. This study has been done in this work and results examining how the accuracy of the solution is affected by the outflow boundary condition are going to be discussed in the next section.

Equations (11) and (13) represent an algebraic system of nonlinear equations, which is solved with a Newton–Raphson iterative scheme. The convergence criterion imposed on the Newton–Raphson iteration was 10^{-6} for velocities and $5 \cdot 10^{-4}$ for pressure. Gauß elimination is used for the inversion of the Jacobian matrix, which is formed by differentiating the residuals R^i_{C} and R^i_{M} with respect to the nodal unknowns u_i, v_i and p_i. In Table I, the coordinates of the mesh are given at every point of the computational domain. The finite element program was written in FORTRAN 77. Time integration was performed with the backward Euler method. At each time step, three iterations were necessary for code convergence. It should be noted that the convective terms of the Navier–Stokes equations are dominant for this flow. However, stabilization of these terms was unnecessary, because the mesh used was irregular and denser at locations around the obstacle where stabilization issues may be of importance. After all, our experience with standard Galerkin finite elements shows that any sort of numerical instabilities may be cured by refining the mesh.

All results presented in the next section are independent of time step and mesh resolution. In order to determine this independence of results due to discretization, the code was run with a

DOI: 10.1002/fld

Table I. Data of computational mesh of Figure 3.

Number of elements	14 645
Number of nodes	59 299
Number of unknowns	133 603
CPU time per iteration	3 min
Computer used	Pentium (R) 4 CPU 2.66 GHz 1.00 GB RAM
Location of obstacle	$14 \leqslant x \leqslant 15$
Height of obstacle	$0 \leqslant y \leqslant 1$
Time step	0.01

x-coordinate

```
−3.0,−2,−1,−0.5,−0.25,−0.125,0.0,0.125,0.25,
0.5,0.75,1,1.25,1.5,1.75,2,2.25,2.5,2.75,
3,3.5,4,4.5,5,5.5,6,6.5,7,7.5,8,8.5,9,9.5
10,10.5,11,11.5,12,12.2,12.4,12.6,12.8,13,
13.1,13.2,13.3,13.4,13.45,13.5,13.55,13.6,
13.65,13.7,13.75,13.8,13.85,13.90,13.95,
13.96,13.97,13.98,13.99,14,14.01,14.02,
14.03,14.04,14.05,14.10,14.15,14.20,14.25,
14.30,14.35,14.40,14.45,14.50,14.55,14.60,
14.65,14.70,14.75,14.8,14.85,14.90,14.95,
14.96,14.97,14.98,14.99,15,15.01,15.02,
15.03,15.04,15.05,15.1,15.15,15.2,15.25,
15.3,15.35,15.4,15.45,15.5,15.6,15.7,15.8,
15.9,16,16.1,16.2,16.3,16.4,16.5,16.6,16.7,
16.8,16.9,17,17.1,17.2,17.3,17.4,17.5,17.6,
17.7,17.8,17.9,18,18.1,18.2,18.3,18.4,18.5,
18.6,18.7,18.8,18.9,19,19.1,19.2,19.3,19.4,
19.5,19.6,19.7,19.8,19.9,20,20.1,20.2,20.3,
20.4,20.5,20.6,20.7,20.8,20.9,21,21.1,21.2,
21.3,21.4,21.5,21.6,21.7,21.8,21.9,22,22.1,
22.2,22.3,22.4,22.5,22.6,22.7,22.8,22.9,23,
23.1,23.2,23.3,23.4,23.5,23.6,23.7,23.8,
23.9,24,24.1,24.2,24.3,24.4,24.5,24.6,24.7,
24.8,24.9,25.0,25.1,25.2,25.3,25.4,25.5,
25.6,25.7,25.8,25.9,26,26.1,26.2,26.3,26.4,
26.5,26.6,26.7,26.8,26.9,27,27.1,27.2,27.3,
27.4,27.5,27.6,27.7,27.8,27.9,28,28.1,28.2,
28.3,28.4,28.5,28.6,28.7,28.8,28.9,29,29.1,
29.2,29.3,29.4,29.5,29.6,29.7,29.8,29.9,30,
31,32,33,34,35,36,37,38,39,40,41,42,43,44,
45,46,47,48,49,50,51,52,53,54,55,56,57,58,
59,60.
```

y-coordinate

```
0,0.01,0.035,0.06,0.085,0.11,0.14,0.2,0.3,
0.35,0.40,0.45,0.50,0.55,0.60,0.65,0.70,
0.75,0.8,0.85,0.9,0.95,0.97,0.98,0.99,1,
1.005,1.01,1.02,1.03,1.04,1.05,1.06,1.1,
1.25,1.5,1.75,2,2.33,2.67,3,4,5,6,7,8,8.5,
8.75,9,9.1,9.2,9.3,9.4,9.5,9.55,9.6.
```


DOI: 10.1002/fld

denser mesh by doubling the number of elements in the x and y direction and with a finer time step by reducing the time step given in Table I to half. The output was compared to the results obtained for the time and space discretization given in Table I. Regarding the accuracy of the mesh discretization, the results are shown in the next section following the discussion of the influence of the outflow boundary conditions.

It should be noted that the Kolmogoroff scale, which is of the order of 0.1 mm, is approximately satisfied in the vicinity of the obstacle. However, as pointed out by Moin and Mahesh [15], accurate results in turbulent flows may be obtained with mesh resolutions which have length scales of the order of magnitude of Kolmogoroff's scales. From a computational point of view, it is irrelevant if theoretical length scales are resolved, as long as the results are independent of the discretization error of the numerical scheme. After all, it may be possible that even mesh resolutions with scales smaller than Kolmogoroff's produce mesh-dependent results, depending on the type of flow under consideration. The ultimate judgement though for the accuracy of computational results is the comparison with the available laboratory experimental measurements and the test whether universal turbulent characteristics are validated, which is discussed in the next section.

5. RESULTS AND DISCUSSION

In the following discussion, mean values of the flow variables are computed in the standard way as

$$\bar{u} = \frac{1}{T} \int_{t_0}^{t_0+T} u \, \mathrm{d}t$$

with $t_0 = 150$, $T = 350$ and u the instantaneous value of the flow variable. The transition period for this flow is 140 dimensionless time units (see Figures 4–7 and 12–15). Additionally, data taken for a period of 350 dimensionless time units are enough, in order for the mean values of the flow to obtain statistically stationary values. At every time step of the calculation, the solution was stored, so that 35 000 numerical data points were available for the analysis of the results. Simpson's rule has been used for the evaluation of the above-mentioned integral. The fluctuations u' are calculated then as

$$u' = u - \bar{u}$$

The instantaneous values u of the flow variables have been obtained from the direct computation of the governing equations with the boundary and initial conditions given in the previous sections. Instantaneous properties, mean values and fluctuations of the flow field are discussed next and their interactions are elucidated.

5.1. Instantaneous streamlines of the flow

Instantaneous streamlines are shown at selected time steps in Figures 4–7. In the beginning of the flow, the recirculation region increases downstream of the obstacle, until it becomes big enough and breaks into two parts. One part is attached to the downstream side of the obstacle and the other part is a vortical structure that travels downstream. As time advances, this phenomenon of growth of the recirculation region until it breaks into two parts continues incessantly, since the flow rate is constant at the inlet.

DOI: 10.1002/fld

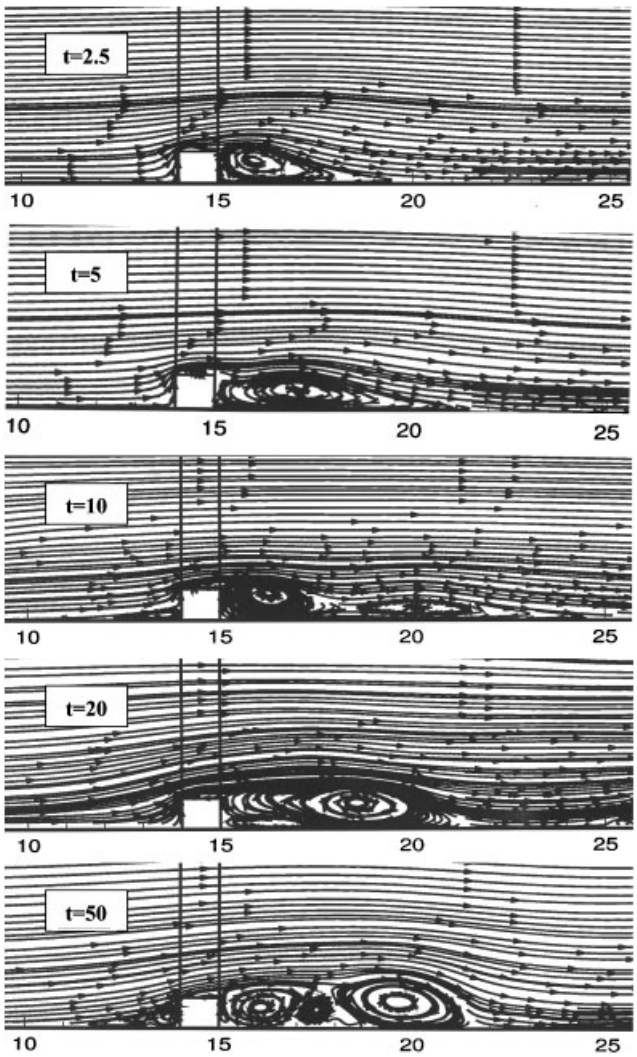

Figure 4. Computed streamlines that describe the development of turbulent flow in the first 50 time units.

The transition period for this flow is depicted in Figures 4 and 5 up to time $t = 140$. During this time, the regular, laminar, initial flow configuration is transformed to a fully developed turbulent flow. In Figure 6, shorter time intervals of the streamline patterns are shown, so that the reader can follow how two consecutive vortices break from the recirculation region downstream of the obstacle and continue travelling. The time needed for one vortex to be generated is between 15 and 20 dimensionless time units. The exact time is going to be calculated later in the discussion of the oscillograms of the fluctuations. Additional streamline patterns are shown up to the last time step of our calculation for this flow in Figure 7.

DOI: 10.1002/fld

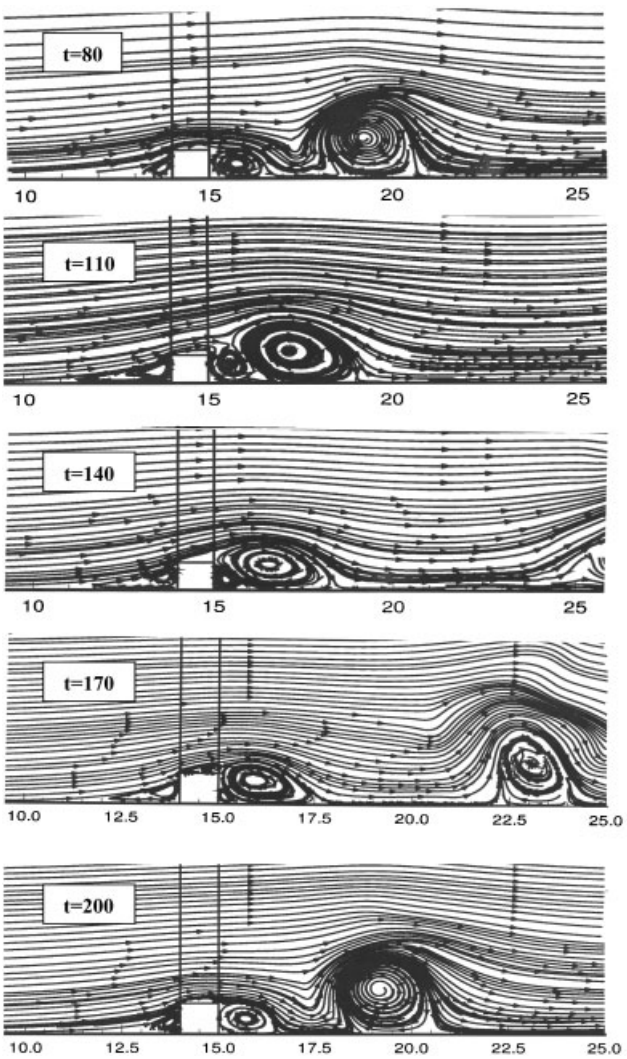

Figure 5. Computed streamlines in the interval from 80 to 200 time units that show the end of the transition from laminar to turbulent flow and the beginning of the generation of the isolated vortices, that travel downstream.

The travelling of the isolated vortices downstream is reminiscent of the von Kármán vortex street as also pointed out by John and Liakos [7], who studied this phenomenon at laminar flow conditions. Due to the constant production of these isolated vortices, a series of four can be observed in the downstream distance of the computational domain, as shown in Figure 8. It should be noted though, that in the case of the flow around a cylinder these vortical structures appear if the flow field is calculated with the velocity of the mean flow. In our study, the vortices appear in the instantaneous snapshots of the streamlines in Figures 4–8, due to the fact that they are produced on the surface of the wall and they move downstream carried by the flow.

DOI: 10.1002/fld

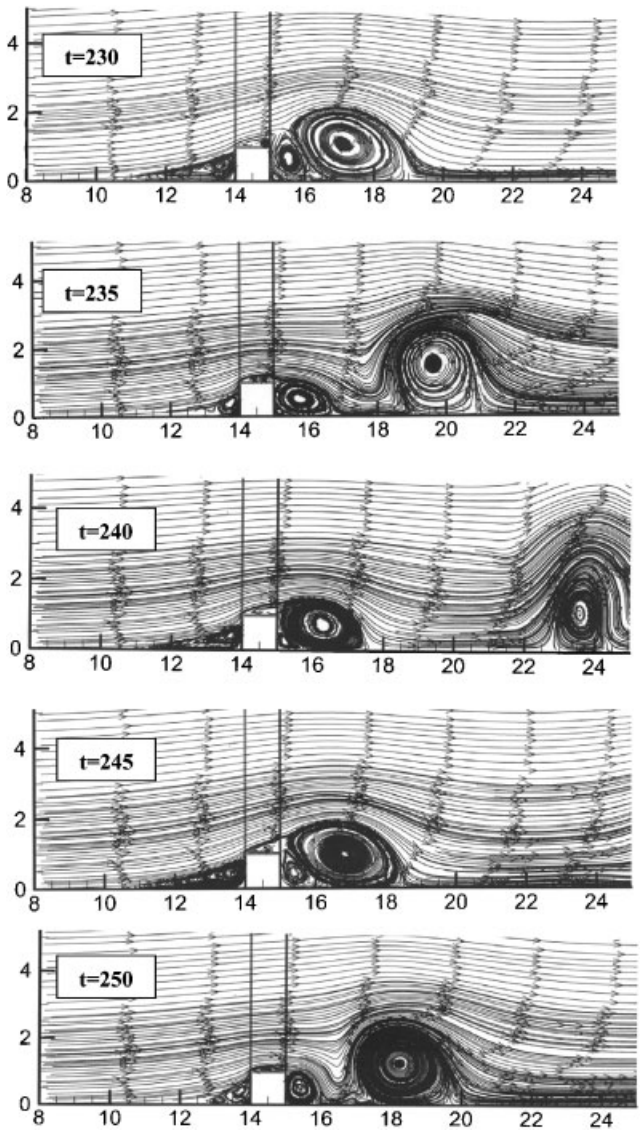

Figure 6. Computed streamlines in the interval from 230 to 250 time units that show how two consecutive vortices emerge from the recirculation region.

This characteristic structure of the turbulent flow field emphasizes the importance of the choice of the correct outflow boundary condition. In Figure 8, five pictures of instantaneous streamline patterns of the whole flow field are depicted. It may be followed how the isolated vortex leaves the computational domain without affecting the solution in the interior. Apart from that test, that justifies the use of the free boundary condition in this work, it is important for the discussion of

DOI: 10.1002/fld

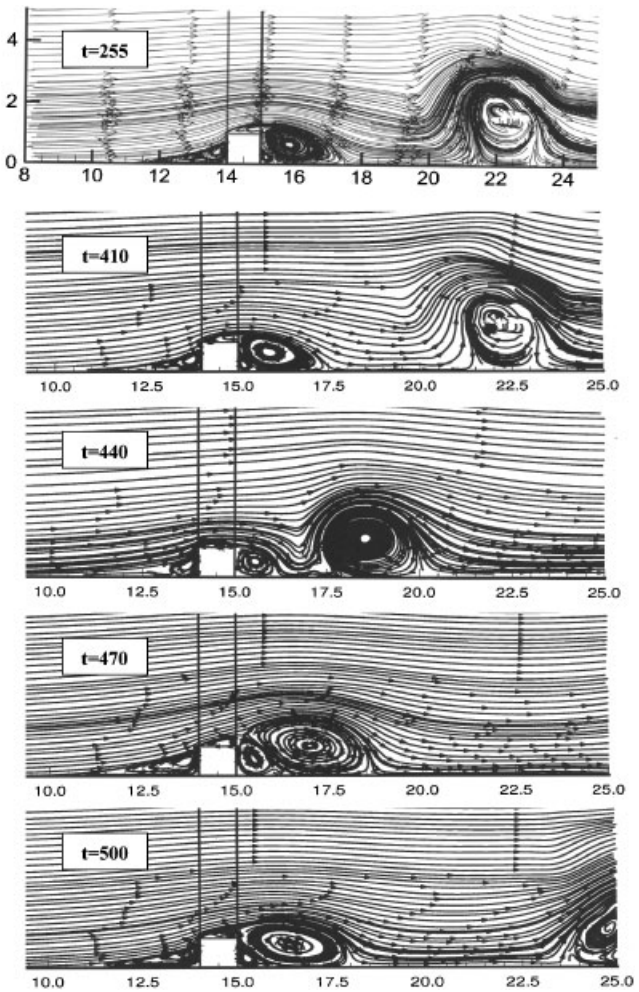

Figure 7. Computed streamlines in the interval from 255 to 500 time units that show the periodic nature of the constant generation of isolated vortices and the consecutive growth of the recirculation region until it breaks again and becomes smaller and grows and so on.

the results that follow to know in detail if and how much the velocity profiles are distorted in the vicinity of the outflow.

For this purpose, the computer code was run with a computational domain 10 units of length shorter than the regular domain given in Figure 1. This procedure is the standard way to investigate whether an outflow boundary condition works well, as thoroughly discussed by Sani and Gresho [25]. The results are shown in Figure 9. The regular domain is termed long domain in that figure, in order to distinguish it from the shorter domain. The profiles of u- and v-velocity of these runs at positions $x = 40, 45, 50$ of the short domain are compared to the corresponding profiles obtained from the long domain at the same x-coordinate. There is some discrepancy of 10% in the

DOI: 10.1002/fld

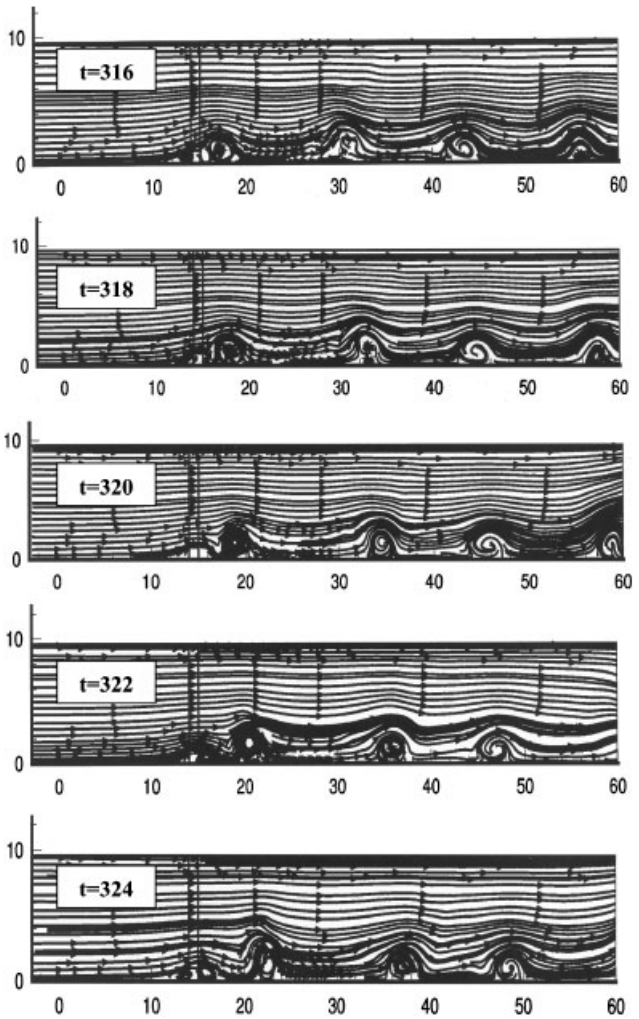

Figure 8. Computed streamlines in the interval from 316 to 324 time units that show how an isolated vortex leaves the computational domain without any distortion of the flow phenomena in the interior.

u- and v-profiles at the exit of the short domain ($x = 50$), which diminishes to 5% for the profiles at $x = 45$. Finally, at 10 units of length upstream of the outflow of the short domain ($x = 40$), the results for the profiles of both velocity components are practically identical. This result means that at least at 10 units of length upstream of the regular domain (at $x = 50$ in Figure 3), the analysis of instantaneous magnitudes of the velocity and its fluctuations are completely unaffected by any unavoidable inaccuracies caused due to the artificial outflow boundary.

It should be noted that the flow phenomena are very intense in the computational domain up to the exit, although the contrary may have been expected as the distance from the downstream side of the obstacle increases. This persistent existence of vortices downstream of the obstacle is

DOI: 10.1002/fld

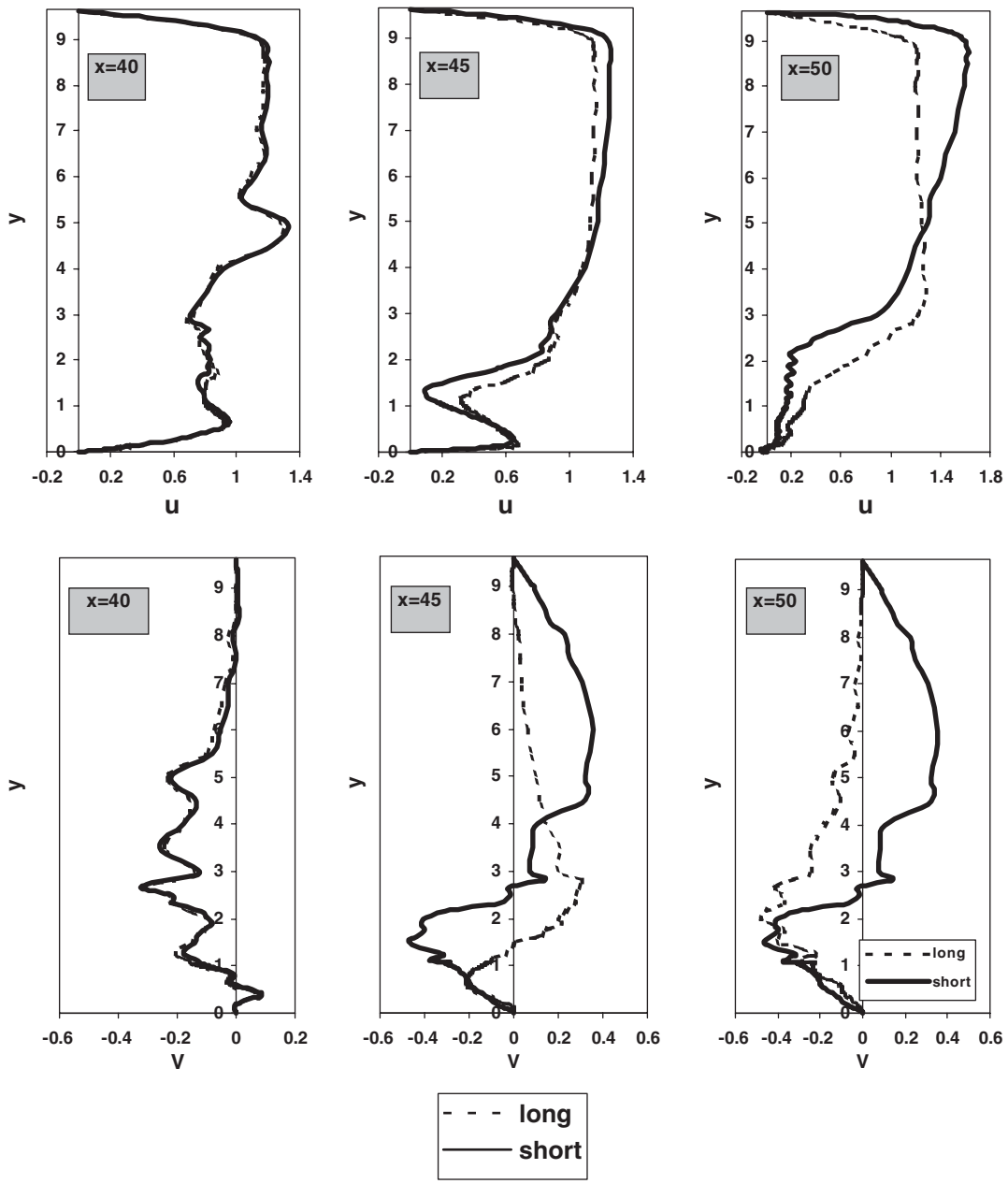

Figure 9. Comparison of u- and v-velocity components at three different locations between the long (60 units of length) and the short (50 units of length) domain that sheds more light to the performance of the free boundary condition at the outflow of the computational domain.

DOI: 10.1002/fld

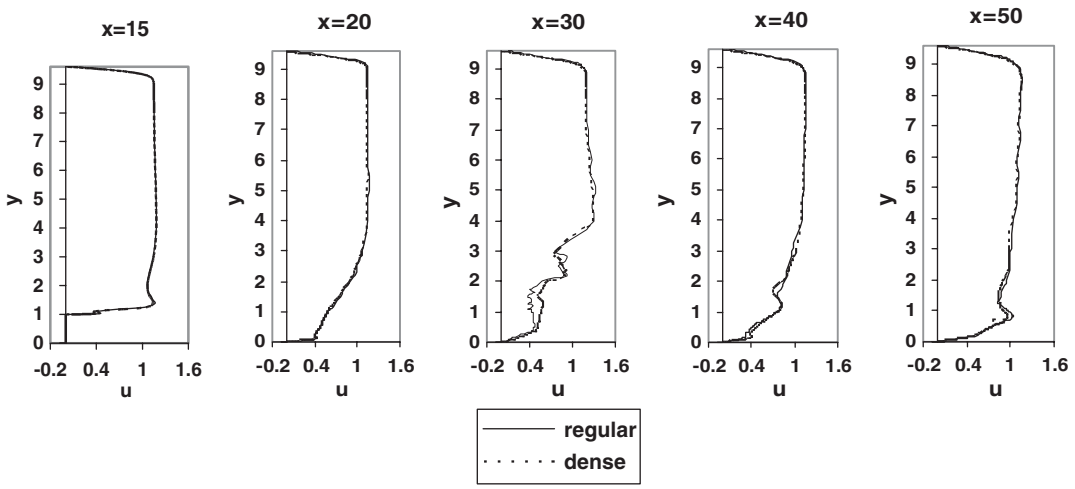

Figure 10. Study of mesh independence. The mesh used in this work is termed regular mesh (see Table I). Dense mesh is the discretization by doubling the elements in both the x- and y-directions of the regular mesh.

analogous to the well-known fact that the von Kármán vortex street continues undisturbed even at 70 diameters downstream the cylinder, as observed by Taneda [33].

From a computational point of view, the outflow should be chosen at a distance where the intensity of the fluctuations and vortical structures diminishes. However, this is not the case for this flow, due to the continuous production of vortices and the nature of turbulence. Other concepts for outflow boundary conditions should be developed for such cases. It is interesting that the free outflow boundary condition performs well for such a flow situation, since this concept has been developed for laminar flow problems and used successfully in other applications [1, 34, 35], where the flow was far from turbulence.

The results of the study of the mesh independency of the numerical solution are shown in Figure 10. Regular mesh is termed the tessellation of the domain given in Table I. Dense mesh is termed the discretization of the domain by doubling the finite elements of the regular mesh in both x- and y-direction. The results for both mesh tessellations are indistinguishable up to $x=20$, that is five units of length downstream of the obstacle. At position $x=30$, there is some discrepancy in the region $0.5<y<3$. The results are again almost indistinguishable at the other x-positions in the figure. The locations shown in Figure 10, have been chosen, because the analysis of the statistical characteristics of turbulence is going to be made at the same x-coordinates at $y=5$ (Figures 12–18). The comparison of the numerical results with the available experimental data is done at locations $x\leqslant 22.1$ (Figures 21–25). That is, in the analysis that follows, all our numerical results are mesh independent. It should be noted that the results of the v and p profiles are analogous to the u profiles shown in Figure 10. The numerical results are also independent of the time step chosen. The discussion of this study is omitted, since, in all cases, the profiles are similar to the profiles at $x\leqslant 20$ of Figure 10. We avoided comparing mesh independence by looking at averaged profiles, since averaging damps the instantaneous picks in the magnitudes of velocities, as is going to be shown in the following discussion of the mean streamlines of the flow.

DOI: 10.1002/fld

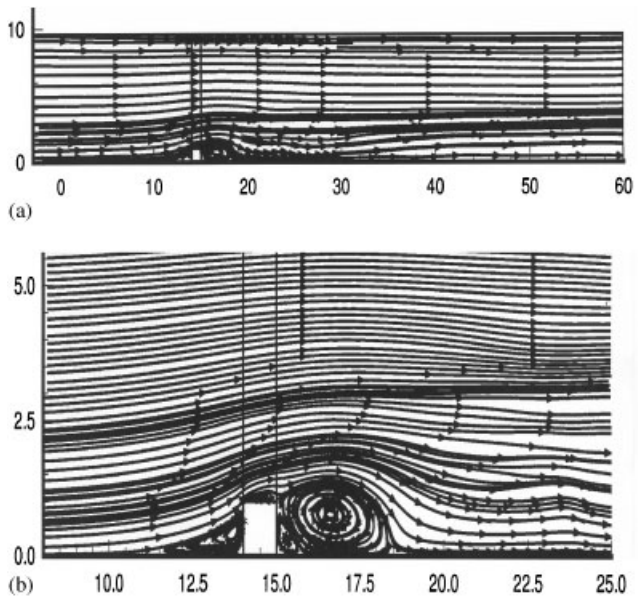

Figure 11. (a) Computed streamlines with the mean values of the velocity components in the whole domain and (b) details of the vortical structures in the vicinity of the obstacle that show how the physics of the flow are completely smoothened if mean properties are considered.

5.2. Mean streamlines of the flow

It is common practice in turbulent research to present results by computing mean values of the flow variables. The streamline pattern of the mean flow field is shown in Figure 11. By comparing this figure with any instantaneous flow field given in Figures 4–8, it is clearly shown that there is a striking difference in the physics. All isolated vortices are completely absorbed in Figure 11 and the recirculation region is smoothened. There is no indication of the intense flow phenomena in the immediate region downstream of the obstacle that cause growth and separation of vortices.

This discrepancy between instantaneous and mean streamline patterns justifies the study of turbulence by means of a direct computation of the Navier–Stokes equations, since flow phenomena may be completely distorted if only mean values of the flow variables are calculated. Certainly, the work of Reynolds, Prandtl and other exceptional engineers, mathematicians and physicists in fluid mechanics has been very influential from late 19th century up to this date, so that any analysis of turbulent calculations even now should refer to some standards, that they established. However, the direct computation of turbulent flows gives—besides laboratory experiments—a deeper insight into the physics of flow phenomena than any other theoretical or computational effort, which is based on the analysis of mean values or statistical properties.

5.3. Velocity fluctuations

Oscillograms of u- and v-velocity fluctuations are shown in Figures 12–15 at various locations of the flow domain. In all these figures, the y-coordinate was kept constant at $y = 5$ and the x-coordinate was varied from 20 to 50. At point ($x = 20$, $y = 5$), which is relatively close to the

DOI: 10.1002/fld

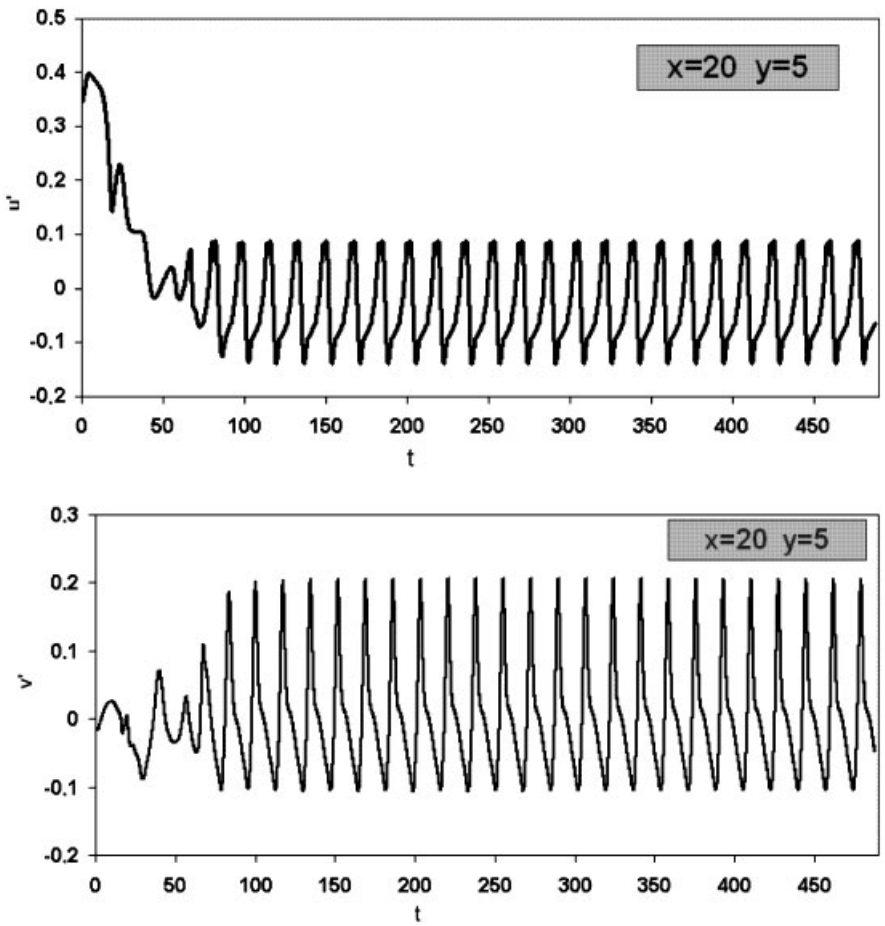

Figure 12. Oscillations of the fluctuations of both velocity components at point ($x = 20$, $y = 5$) of the computational domain. The signals seem to be almost periodic after the transition period from the initial laminar flow condition to fully developed turbulence.

obstacle (5 units of length downstream of the trailing edge), the fluctuations are completely regular after a certain transition period of 75 units of time. This regularity in the signal is due to the constant generation of vortices downstream of the obstacle, as shown in Figures 4–8. The only source of turbulence here is the disturbance of the flow due to the presence of the obstacle. It is expected that turbulence is still undeveloped in the immediate vicinity of the obstacle. The computed result should be an almost periodical oscillogram of the fluctuations for both velocity components, as is actually shown in Figure 12. The period of oscillation is 16.7 dimensionless time units. This value corresponds to the time taken for one vortex to break from the recirculation region, which has already been approximately estimated in the discussion of Figure 6.

Further downstream at point ($x = 30$, $y = 5$) in Figure 13, the oscillograms of the fluctuations are almost as regular as in the previous picture, although there is a certain randomness in the minima and maxima of the signal especially for the fluctuation of the v-component of the velocity.

DOI: 10.1002/fld

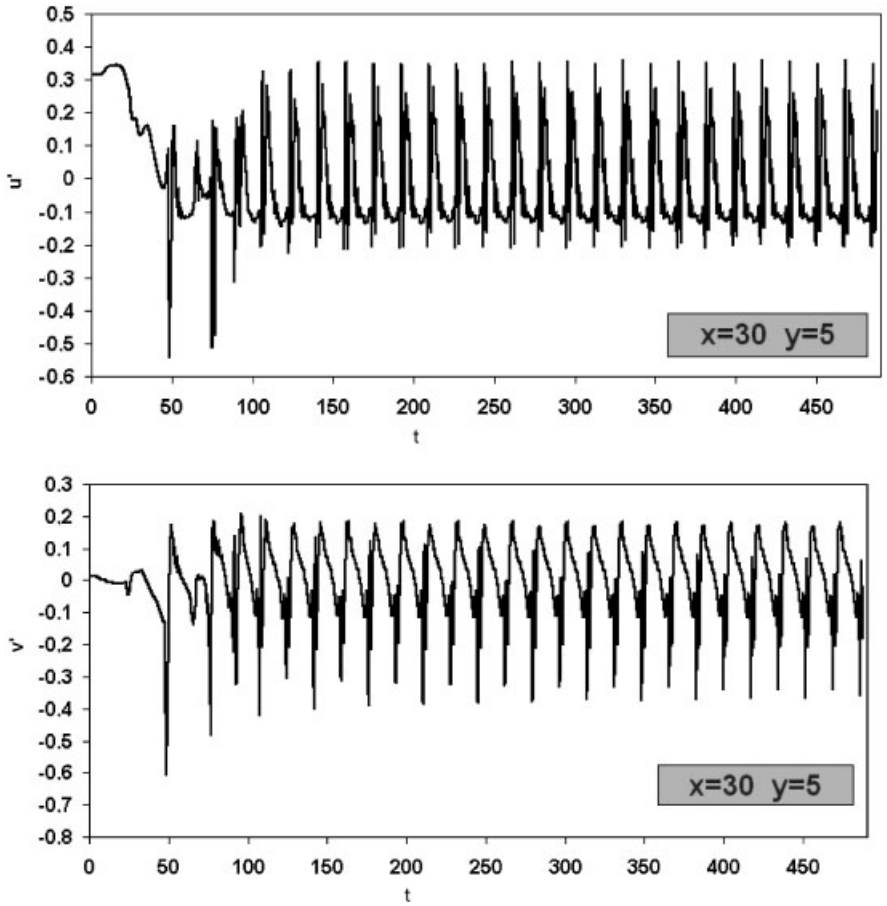

Figure 13. Oscillations of the fluctuations of both velocity components at point $(x = 30, y = 5)$ of the computational domain. The signals exhibit a weak randomness in the maxima and the minima after the transition period.

Another difference with Figure 12 is that the transition period lasts about 100 units of time, since it takes more time for the initial disturbance to reach this point.

In Figures 14 and 15 at points $(x = 40, y = 5)$ and $(x = 50, y = 5)$, respectively, the situation is completely different. The flow develops turbulent characteristics in a much more pronounced fashion. The result is a randomness in the oscillograms of the velocity fluctuations superimposed on the periodicity due to the steady generation of vortices. This randomness is exhibited in the acanonical variation of the minima and the maxima of the amplitude of the oscillations. The period of the oscillation is undisturbed, though, as it should be, due to the periodic nature of the flow at this Reynolds number. Additionally, randomness is also observed within each period of oscillation, where the pattern of the fluctuations is different and acanonical as well. This difference in the pattern may not be obvious at a first glance, due to the dominant periodical nature of the signal. However, the randomness in the pattern exists and gives the message that turbulence develops as

DOI: 10.1002/fld

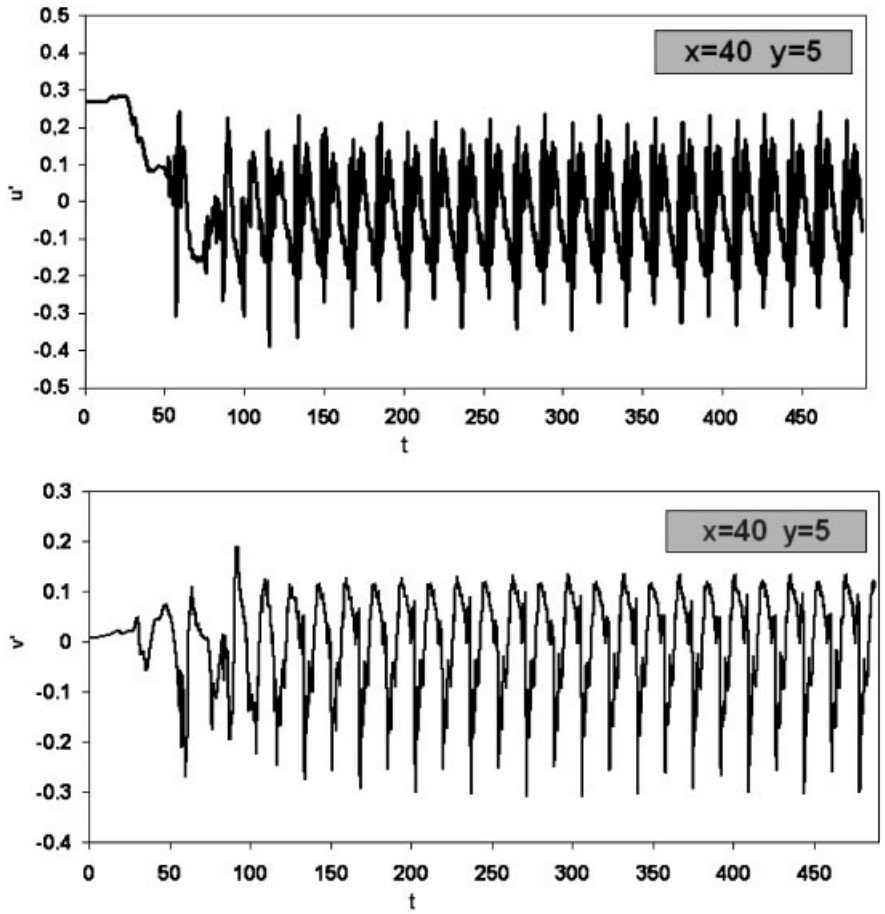

Figure 14. Oscillations of the fluctuations of both velocity components at point ($x = 40$, $y = 5$) of the computational domain. The signals exhibit a stronger randomness in the maxima and the minima as the flow continues downstream.

the flow is distanced from the obstacle. Especially Figure 15 is reminiscent of the signals taken by many experimentalists over the last 80 years and shown in standard books of turbulence [36, p. 499; 37, p. 28; 38, p. 12], in order to invoke the intuition of the reader about the complicated nature of turbulent flow and justify the attitude of many workers in the field towards a statistical analysis of turbulence.

In this work, it is shown that deterministic spatiotemporal chaos is predicted by directly solving the Navier–Stokes equations. To the best of our knowledge, this kind of oscillograms is shown for the first time from a computational analysis. So far, even in books dealing with chaos, chaotic behaviour has been limited to the subject of solving equations, where the dependent variables are only a function of time (e.g. [39]). It should be also noted that this behaviour of velocity fluctuations at the points shown in Figures 12–15 is representative of any other point in the flow domain with coordinates (x, y_0), where y_0 is kept at a constant value.

DOI: 10.1002/fld

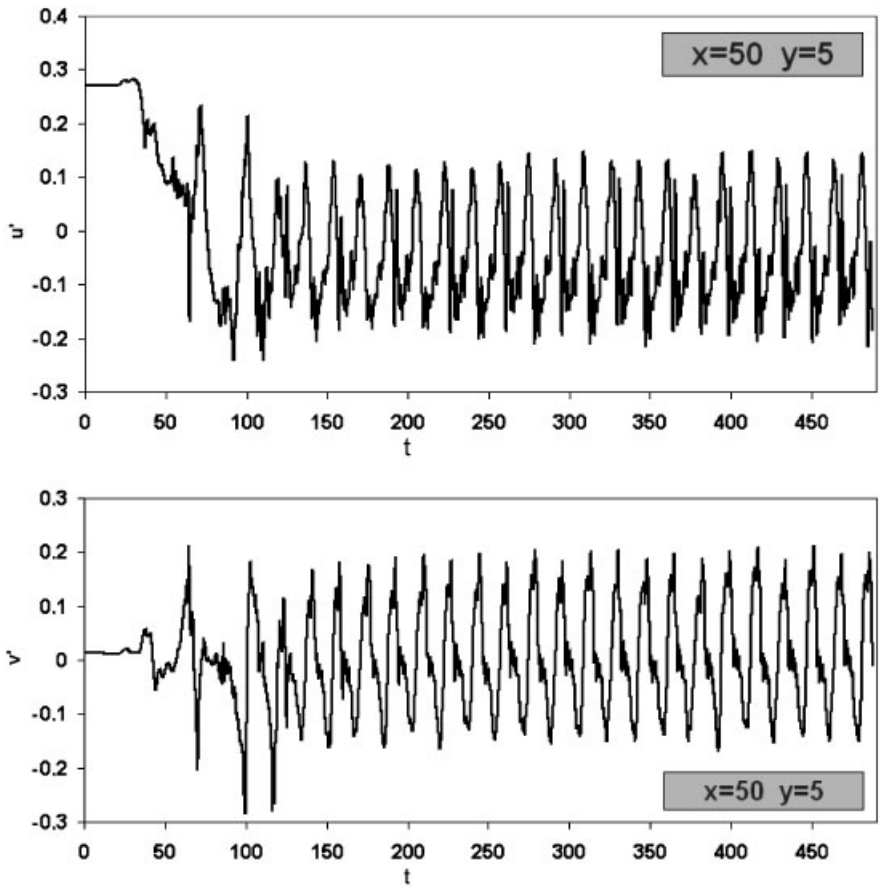

Figure 15. Oscillations of the fluctuations of both velocity components at point ($x = 50$, $y = 5$) of the computational domain. The signals exhibit a total randomness which is a fundamental characteristic of turbulence.

5.4. Energy and enstrophy spectra

It is customary in turbulent research to study the energy and enstrophy spectra of the instantaneous values of velocities and vorticity. Especially, the energy spectrum has been the subject of extensive experimental investigation and has led to an empirical law that has been verified by the deeply influential work of Kolmogoroff, as thoroughly discussed by Frisch [37]. Batchelor [13] and Kraichnan [11] extended these ideas to two-dimensional turbulence. They found that the energy spectrum follows both the $-\frac{5}{3}$ power law of three-dimensional turbulence (called inverse energy cascade in the terminology of two-dimensional turbulence) and the -3 power law, which has been attributed to a forward enstrophy cascade. Additionally, they studied the enstrophy cascade and predicted a -1 power law for the dependency of enstrophy with respect to the frequency of the spectrum.

The energy spectra are shown in Figures 16 and 17. They have been calculated at the same points as the oscillograms of the velocity fluctuations in Figures 12–15 using a specially developed

DOI: 10.1002/fld

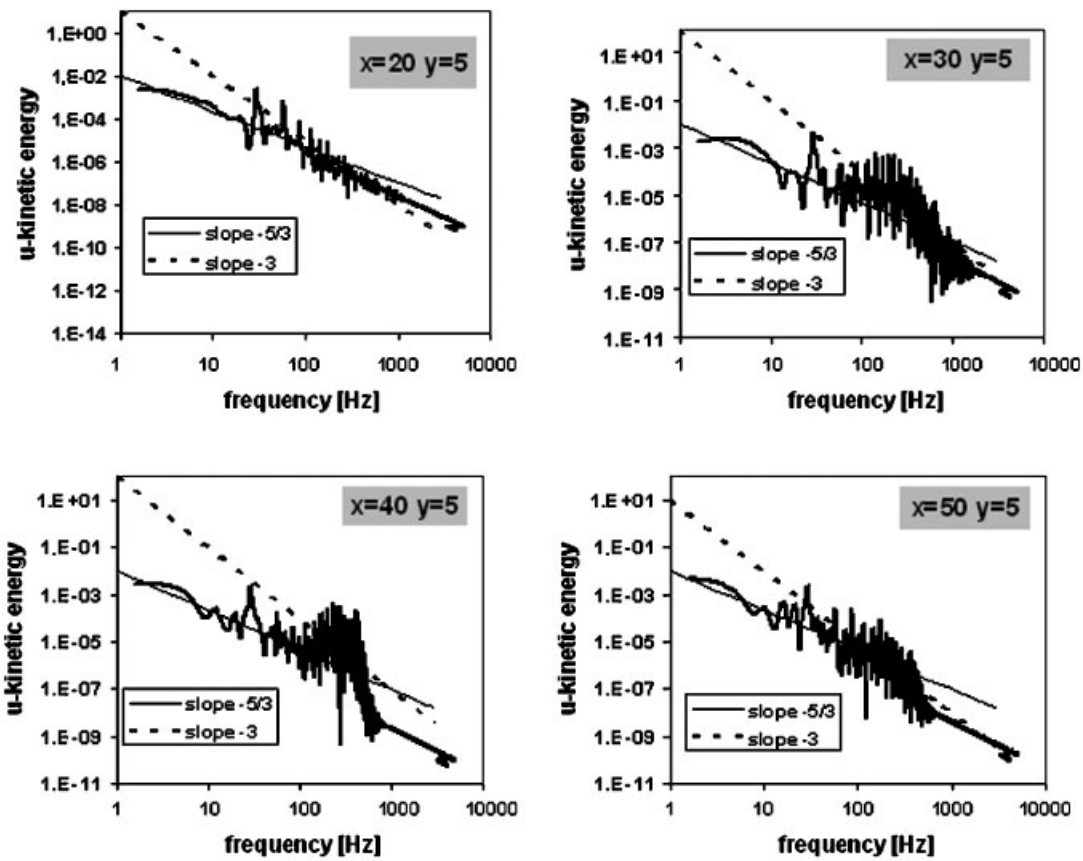

Figure 16. Energy spectra of the kinetic energy of the u-velocity component at four different locations of the computational domain. The calculations have been performed with the commercial program Labview. The dual cascade of two-dimensional turbulence is validated.

computer code based on LabView, the commercial data processing computer software provided by the National Instruments Corporation. A common characteristic of all the graphs in these figures is the spike at 30 Hz, which is attributed to the periodical nature of the generation of vortices downstream of the obstacle. This frequency corresponds to the period of oscillations in Figures 12–15, which is 16.7 dimensionless time units. The reference time h/U_0 is 1.96 ms, so that the period of oscillations obtains the value 32.88 ms. Finally, the inverse of the period is 30.4 Hz, which is the frequency of the spike. This agreement between the observations of the instantaneous streamline patterns, the computation of the oscillograms of the velocity fluctuations and the spectral analysis of these signals provides an additional argument for the reliability of the numerical results of this work.

In Figure 16, the energy spectrum of the u-velocity at point ($x = 20$, $y = 5$) has strong dependencies on both the $-\frac{5}{3}$ and the -3 power law of the frequency. As the flow continues downstream, the $-\frac{5}{3}$ power law appears in a much wider frequency range than the -3 power law especially at point ($x = 40$, $y = 5$). In Figure 17, the energy spectrum of the v-velocity component at point

DOI: 10.1002/fld

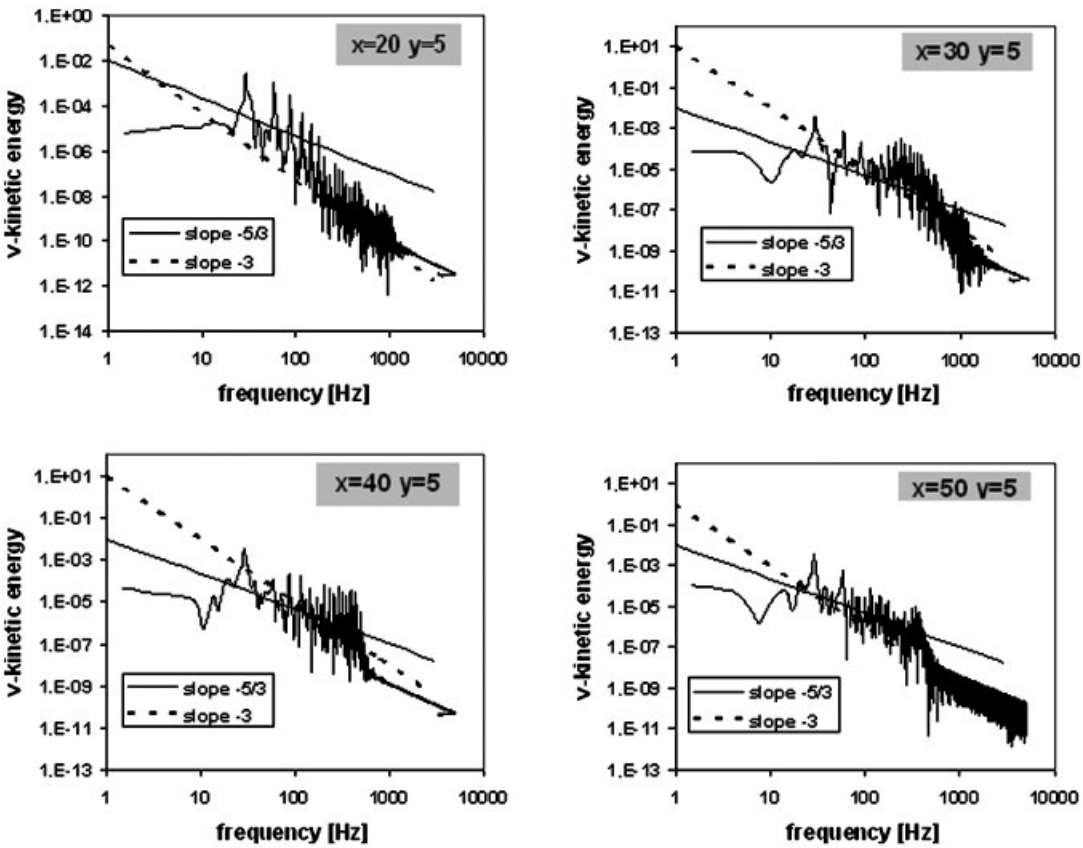

Figure 17. Energy spectra of the kinetic energy of the v-velocity component at four different locations of the computational domain. The calculations have been performed with the commercial program Labview. The dual cascade of two-dimensional turbulence is validated.

($x = 20$, $y = 5$) shows a clear -3 dependency on frequency of almost two orders of magnitude while the $-\frac{5}{3}$ dependency is limited to the region from 30 to 100 Hz. As the flow continues downstream, the dependency of the energy spectrum on frequency is equally divided in both the $-\frac{5}{3}$ and the -3 power law. In any case, the dual cascade of two-dimensional turbulence is clearly demonstrated in all the results of Figures 16 and 17, even though the velocity fluctuations show that turbulence is less pronounced up to point ($x = 30$, $y = 5$).

The enstrophy spectra for this flow are shown in Figure 18 at the same points as the energy spectra. The enstrophy was calculated as one half of the square of vorticity. At point ($x = 20$, $y = 5$), the -1 power law in the decay of enstrophy extends more than one order of magnitude. Up to point ($x = 40$, $y = 5$), this decay is gradually limited to a narrower region. Further downstream, the -1 power law covers again one order of magnitude in the frequency range at point ($x = 50$, $y = 5$). The agreement of the results of the spectral analysis of this work with theoretical results of two-dimensional turbulence confirms the accuracy of the numerical predictions. The slopes $-\frac{5}{3}$ and -3 are included in Figures 16–18, so that the reader may estimate how far or close is the frequency dependence of the kinetic energy from these well-known laws.

DOI: 10.1002/fld

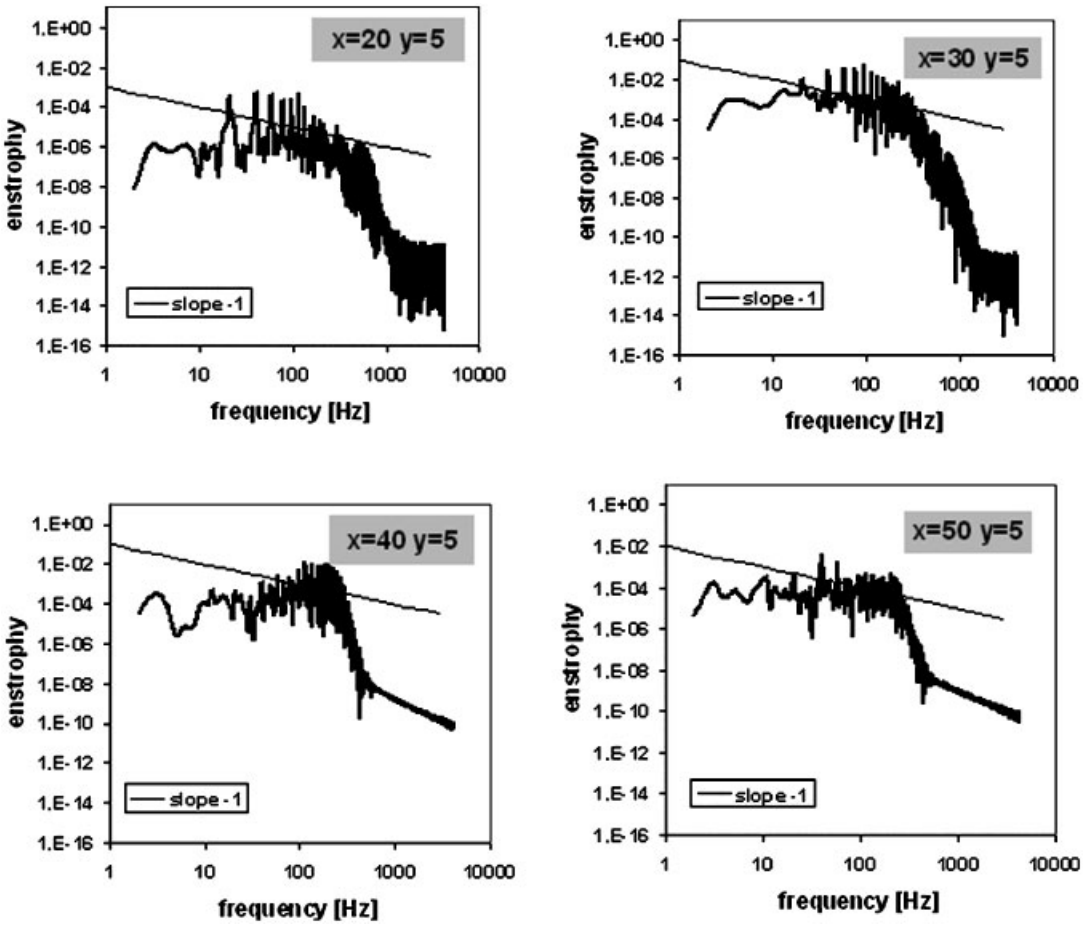

Figure 18. Enstrophy spectra at four different locations of the computational domain. The calculations have been performed with the commercial program Labview. The decay of enstrophy with the -1 power law validates the direct enstrophy cascade of two-dimensional turbulence.

5.5. *Statistical properties of the flow*

Correlation functions are useful tools in studying the spatial structure of turbulence from a statistical point of view. Three correlation functions are calculated in this work with the following definitions:

$$R(\tau) = \frac{1}{T} \frac{\int_{t_0}^{t_0+T} u'(t)u'(t+\tau)\,\mathrm{d}t}{\overline{u'^2}(t)}, \quad R_u(y) = \frac{1}{T} \frac{\int_{t_0}^{t_0+T} u'(x, y_0)u'(x, y_0+y)\,\mathrm{d}t}{\overline{u'^2}(x, y_0)}$$

$$R_v(y) = \frac{1}{T} \frac{\int_{t_0}^{t_0+T} v'(x, y_0)v'(x, y_0+y)\,\mathrm{d}t}{\overline{v'^2}(x, y_0)}$$

DOI: 10.1002/fld

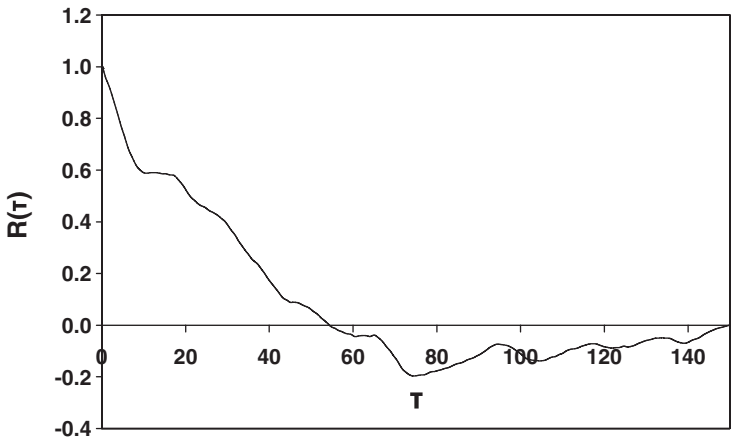

Figure 19. The Eulerian autocorrelation function at point ($x = 50$, $y = 5$) calculated from the computed fluctuations of the u-velocity component.

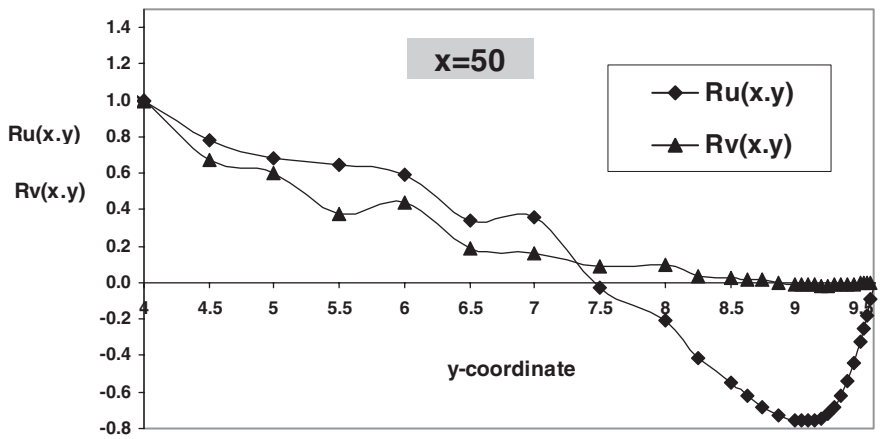

Figure 20. The longitudinal $R_u(y)$ and lateral $R_v(y)$ cross-correlation functions calculated from the computed fluctuations of the u- and v-velocity components, respectively, with fixed point ($x = 50$, $y_0 = 4$) and variation along the y-coordinate of the computational domain up to the upper wall of the wind tunnel.

$R(\tau)$ is the Eulerian autocorrelation function that relates the fluctuation of the u-velocity component at a certain point of the flow domain to the fluctuation of the same velocity component at the same point at a later time. $R_u(y)$ is the longitudinal correlation function that relates the fluctuation of the u-velocity component at a certain point of the flow field and time to the fluctuation of the same velocity component at a different point in the y direction of the flow field at the same time. $R_v(y)$ is the lateral correlation function that relates the fluctuation of the v-velocity component in the corresponding way as $R_u(y)$. The values of t_0 and T have been given in the beginning of this section. All three integrals have been calculated with Simpson's rule.

DOI: 10.1002/fld

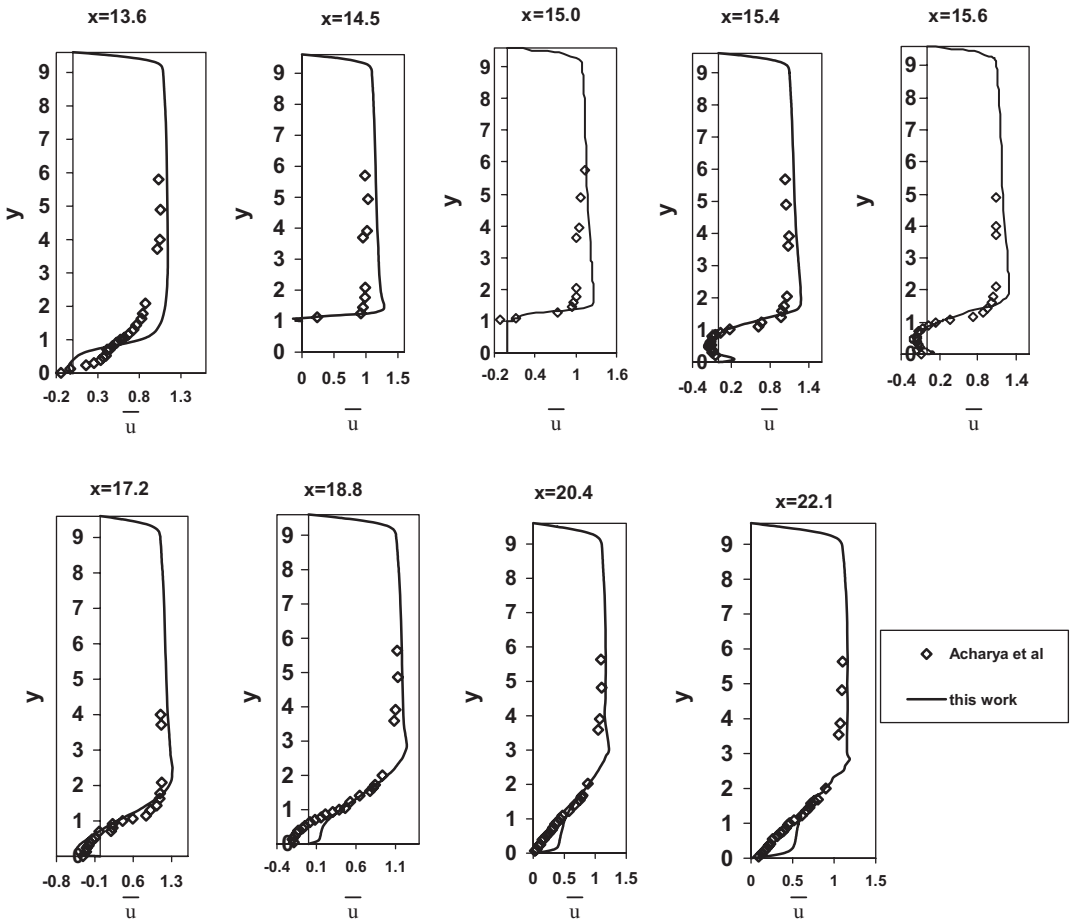

Figure 21. Comparison of calculated mean u-velocity profiles *versus* laboratory data obtained by Acharya *et al.* (1994) at various locations of the computational domain.

The autocorrelation function $R(\tau)$ at point $(x = 50, y = 5)$ is shown in Figure 19. The dimensionless time difference τ goes up to 150 time units. $R(\tau)$ has been evaluated at each time step yielding 15 000 points for the calculation of the curve in Figure 19. The autocorrelation function starts at 1, diminishes gradually, obtains negative values and finally tends to zero. This is a typically measured curve indicative of the randomness of the signal, which has already been observed in Figure 15.

The longitudinal and lateral correlation functions at point (x=50, y_0=4) are shown in Figure 20. The variation in the y-coordinate goes up to the upper wall of the wind tunnel of the computational domain (see Figure 1). Both correlation functions start from 1 and gradually diminish. The function $R_u(y)$ obtains appreciable negative values like $R(\tau)$ and finally both cross-correlations become zero at the wall due to the no-slip boundary condition there. In the literature [36, p. 579; 40, p. 556], it is stated that the analysis depicted in Figure 20 is rarely done experimentally, because many

DOI: 10.1002/fld

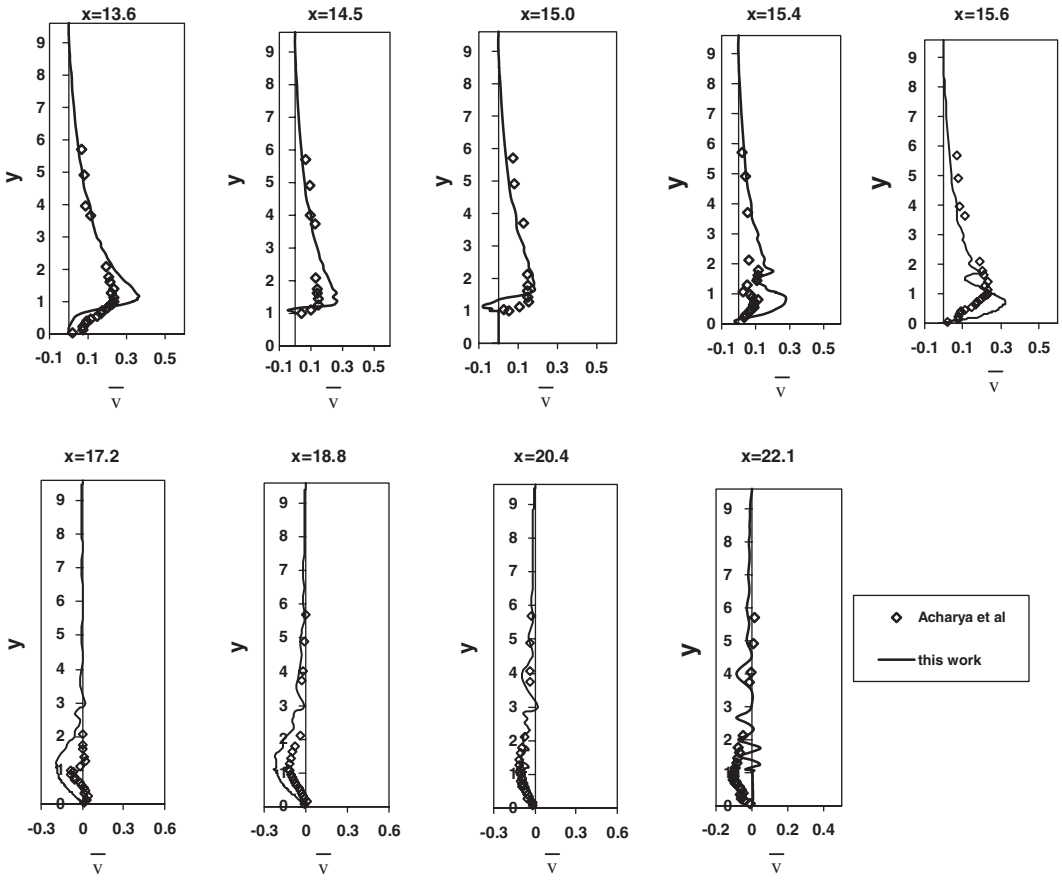

Figure 22. Comparison of calculated mean v-velocity profiles *versus* laboratory data obtained by Acharya *et al.* (1994) at various locations of the computational domain.

measurements are required. However, in the direct computation of turbulent flows this analysis is as straightforward as the calculation of autocorrelation functions, since at every time step of the computation all values of the flow variables in the flow field are obtained, stored and postprocessed as desired.

Although, all three correlation functions are unable to contribute to the understanding of the physics of turbulence, they provide an accurate test for the quality of the computational results. These functions simply examine whether events that take place spatially or temporally away from a fixed point in space or time correlate in an increasingly fading fashion, as it should actually be for a random process, according to common sense. The computational results of this work satisfy this requirement of statistical analysis and verify the chaotic behaviour of the oscillograms of the velocity fluctuations shown in Figures 12–15.

The results of the statistical analysis along with the spectra are consistent with the chaotic nature of the oscillograms in Figures 12–15, which proves, that the tessellation of the domain is adequate for this flow. Certainly, by studying this flow at even higher Reynolds numbers, the

DOI: 10.1002/fld

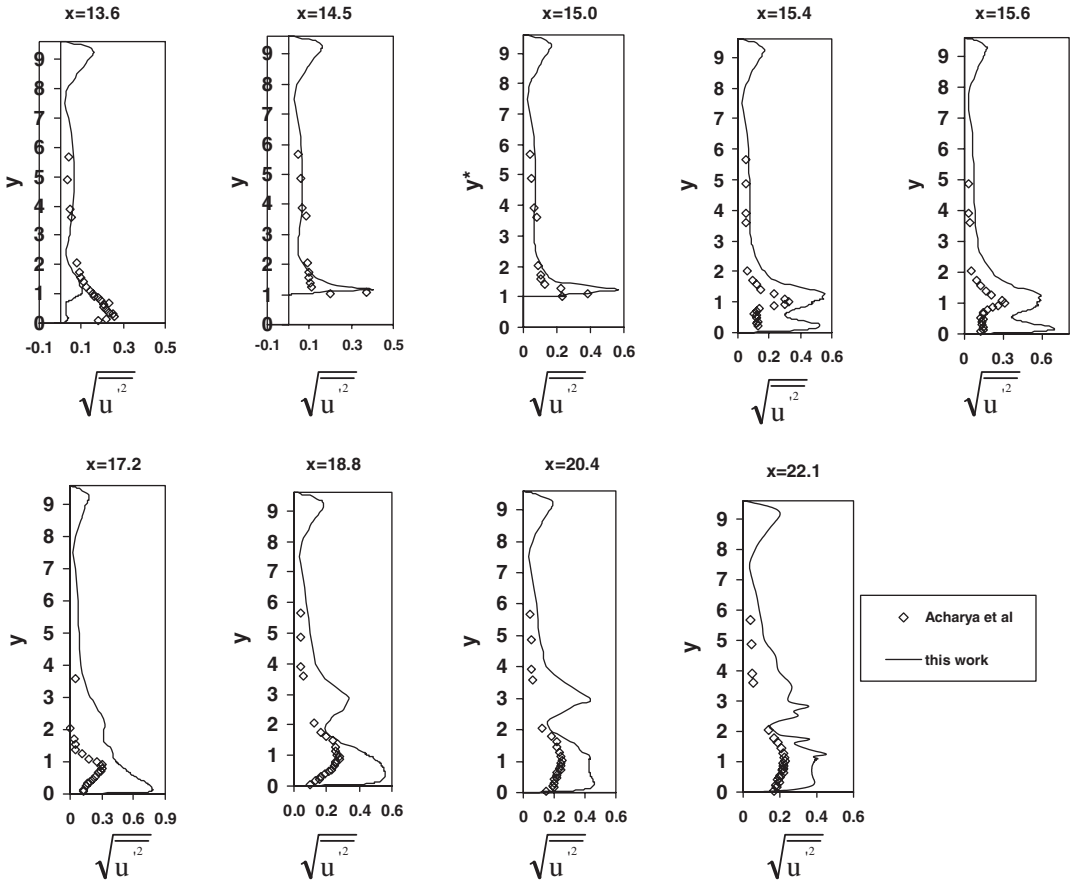

Figure 23. Comparison of calculated root mean square u-velocity profiles *versus* laboratory data obtained by Acharya *et al.* (1994) at various locations of the computational domain.

chaotic behaviour of turbulence may be revealed in a much more profound way. However, since the calculations in this work take more than three months to be completed with the current available means of the authors and since experimental results are missing at higher Reynolds numbers, this analysis is going to be the subject of a future paper.

5.6. Comparison with the laboratory experimental data

The mean profiles of the u- and v-velocity components as well as the root mean square profiles of the fluctuations of velocity along with the Reynolds stress term $\overline{u'v'}$ are shown in Figures 21–25. The corresponding laboratory data taken by Acharya *et al.* [5] are shown in the same figures.

The agreement of the computational results is very good with the experimental data in Figure 21 up to position $x = 17.2$ of the flow domain. Further downstream, there is some discrepancy in the

DOI: 10.1002/fld

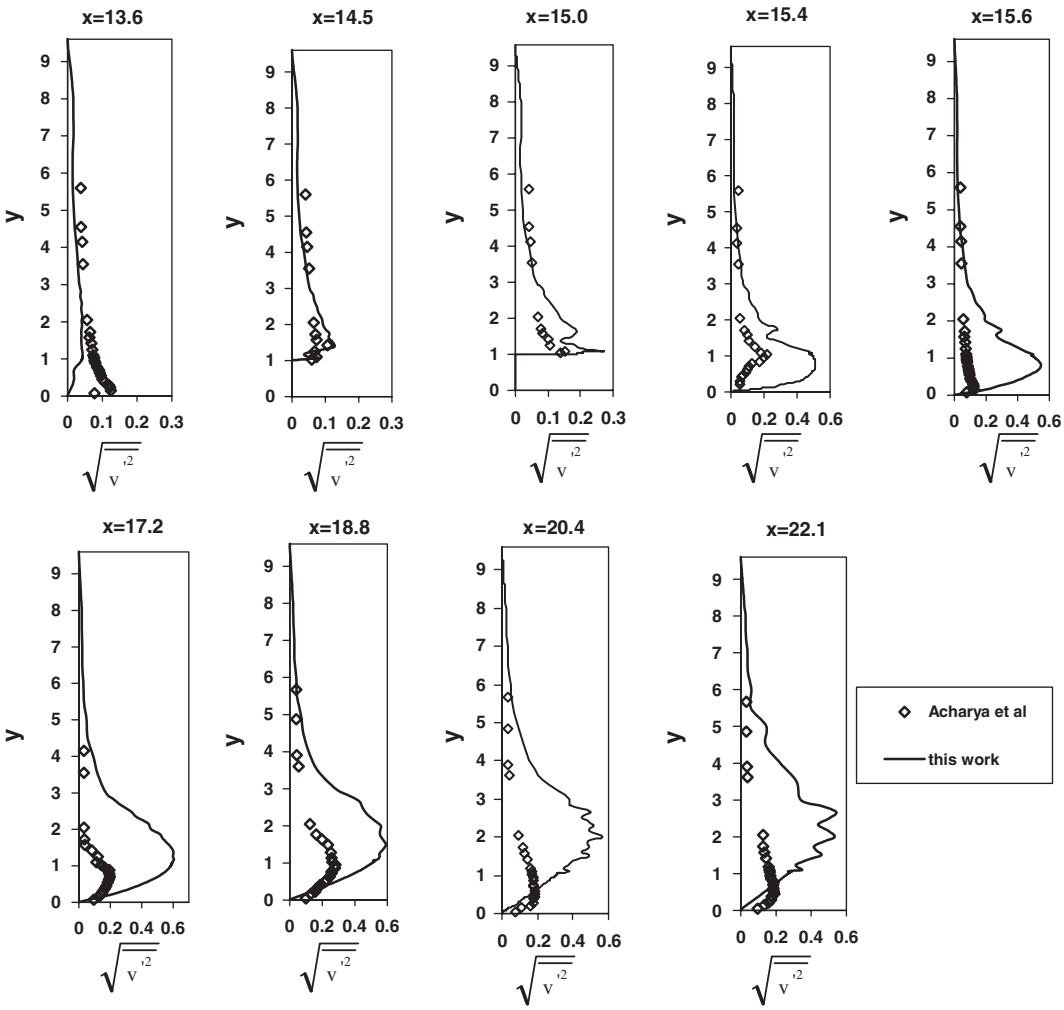

Figure 24. Comparison of calculated root mean square v-velocity profiles *versus* laboratory data obtained by Acharya *et al.* (1994) at various locations of the computational domain.

recirculation region. The quality of agreement in the $\bar{v}$ velocity profile varies depending on the position of the flow, as shown in Figure 22. The comparison is good at positions over the obstacle and downstream at $x = 20.4$. Although the discrepancy is more than 10% in the rest of the profiles, especially at $x = 15.4$, the trend is the same in both studies.

The comparison of the calculated root mean square terms $\overline{u'^2}$ and $\overline{v'^2}$ in Figures 23 and 24 with the experimental results shows an even bigger deviation at positions downstream of the obstacle, although the agreement is relatively good at positions $x = 14.5$ and 15. However, the trend between numerical and experimental results is the same, as in Figure 22. Finally, the comparison of the Reynolds stresses is depicted in Figure 25. Downstream of the obstacle, the discrepancy between

DOI: 10.1002/fld

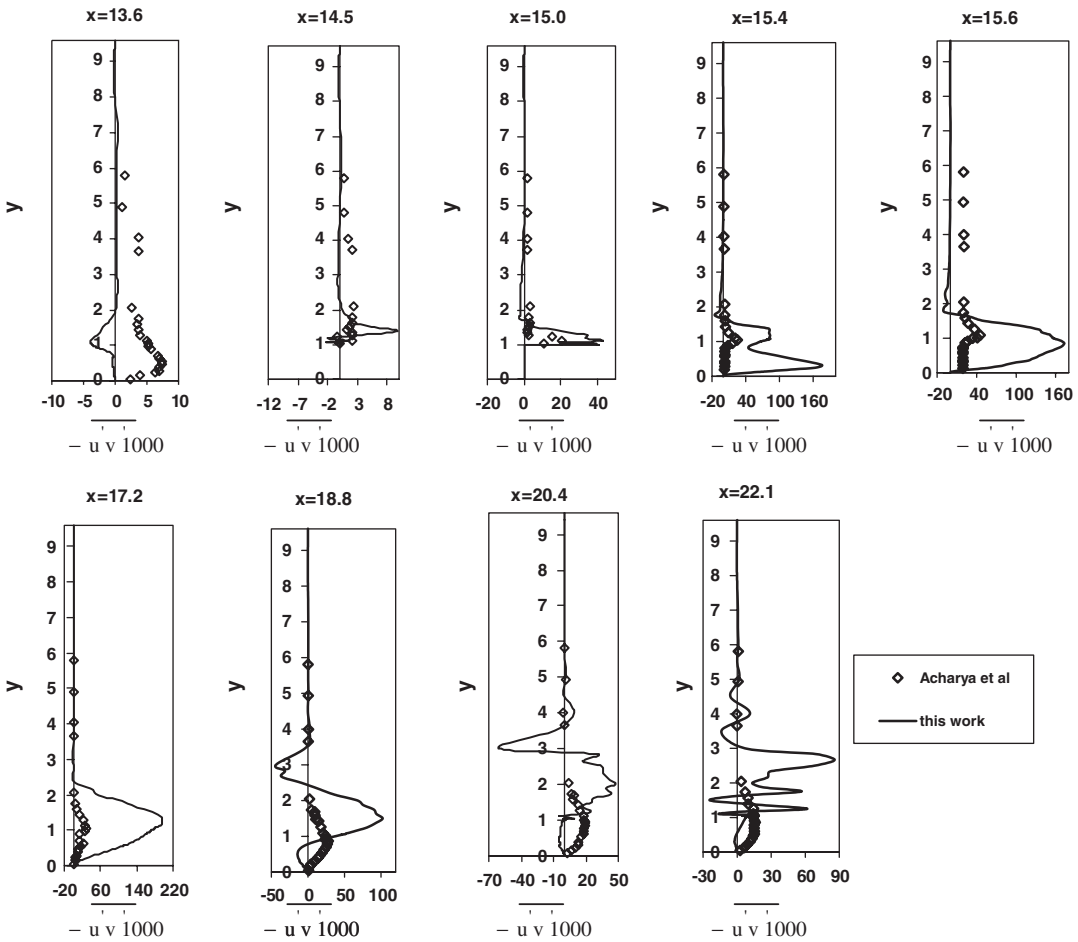

Figure 25. Comparison of calculated Reynolds stress term $\overline{u'v'}$ *versus* laboratory data obtained by Acharya *et al.* (1994) at various locations of the computational domain.

numerical and experimental results is of the same order of magnitude as with the rms values. Again, the trend is the same in the profiles of both works.

This disagreement between numerical and experimental results may be attributed to the complications encountered in measuring the fluctuations in the recirculation region, considering also the small size of the actual experimental set-up. After all, this work examines many issues of turbulence and reproduces fundamental and universal characteristics of at least equal importance as the findings of the laboratory experiments. Additionally, any three-dimensional effects in the actual laboratory experiment are absent in our study of two-dimensional turbulence. This fact may also explain the strong wiggles in Figures 23–25 of the numerical results as opposed to the smooth profiles in the experiments, since the third dimension absorbs some strength of the fluctuations of a two-dimensional numerical experiment.

DOI: 10.1002/fld

6. CONCLUSIONS

In this work, the two-dimensional turbulent flow over a surface-mounted obstacle has been studied numerically with the aim of computing fundamental turbulent characteristics. The computational domain has been designed as close as a laboratory experiment, that may be performed in a wind tunnel. The Navier–Stokes equations have been solved directly with standard Galerkin finite elements at a Reynolds number of 12 518 with respect to the height of the wind tunnel. The computer code yields the instantaneous values of velocities and pressure at every time step of the calculation. In this way, it is permitted to follow the flow phenomena as they evolve from the transition period to fully developed turbulence.

The study of instantaneous streamline patterns of the flow field reveals a continuous generation of vortices that emerge from the breakup of the recirculation region downstream the obstacle. The streamline patterns computed from mean values of the velocities show a smooth flow that dumps the intensity of the actual physics. Oscillograms of the velocity fluctuations confirm the periodic nature of the flow and exhibit the chaotic behaviour of turbulence. The analysis of energy spectra yield the double cascade, which is a characteristic of two-dimensional turbulent flow. The decay of enstrophy with respect to the frequency of the spectrum follows the -1 power law. The computation of the autocorrelation function along with the longitudinal and lateral correlation functions yields the expected result that events far from a fixed point in space or time correlate in a fading fashion. This statistical analysis of the velocity fluctuations verifies the chaotic nature of the flow and confirms the randomness in the patterns of the computed oscillograms. Finally, the comparison of the numerical results with available laboratory experimental data shows qualitatively the same trend in the profiles of both mean velocity profiles as well as root mean square fluctuations and Reynolds stresses, while, quantitatively, the agreement varies depending on the position where the measurements were taken. This study can be extended to three dimensions in a straightforward way.

Apart from the originality of the results of this work, there are some fundamental computational issues which are treated here in a different way than the usual approach in the direct computation of turbulent flows, although some of these concepts are common practices in the direct simulation of transient laminar flows:

(a) The choice of initial condition, where a laminar flow solution is peaked, has been verified with laboratory measurements. The transition to turbulence is the additional information, that has been acquired from this study, and is the topic of a different paper of the authors [8].
(b) The choice of inflow boundary condition, where the flow rate is simply imposed with an undisturbed uniform velocity profile. This inlet condition follows as a consequence of the choice of initial condition. This way, turbulence is generated due to the presence of the obstacle as it actually happens in the real world if any disturbance from noise is excluded.
(c) The choice of outflow boundary condition, where the free boundary condition has been used in a turbulent flow along with the weighted residual formulation of the Navier–Stokes equations. It has been shown, how the vortical structures leave the computational domain without any distortion of the flow in the interior.

It should be noted that choices (a) and (c) are treated for the first time in a direct computation of turbulent flow.

Finally, the finite element method used in this study is seldom chosen in the analysis of turbulent flows, although the numerical results are as reliable as those obtained from other numerical schemes.

DOI: 10.1002/fld

Actually, results from finite element calculations are missing in recent review articles dealing with the direct numerical simulation of turbulent flows in two and three dimensions.

The results of this work may be useful in two ways: on the one hand, to colleagues who are engaged in the study of chaos that emerges from two-dimensional turbulence and on the other hand to colleagues who are engaged in the direct numerical simulation of turbulent flow and are interested in applying the alternative approach to initial and boundary conditions proposed here. Another challenge would be the use of the primitive variable formulation of the Navier–Stokes equations in the study of flows with meteorological interest.

ACKNOWLEDGEMENTS

The computation of the energy and enstrophy spectra was a courtesy of colleague G. A. Sideridis. Financial support for this work has been granted by the Office of the Hellenic Foundation for Research (Program: ARCHIMEDES).

REFERENCES

1. Fragos VP, Psychoudaki SP, Malamataris NA. Computer-aided analysis of flow past a surface-mounted obstacle. *International Journal for Numerical Methods in Fluids* 1997; **25**:495–512.
2. Larichkin VV, Yakovenko SN. Effect of boundary-layer thickness on the structure of a near-wall flow with a two-dimensional obstacle. *Journal of Applied Mechanics and Technical Physics* 2003; **44**:365–372.
3. Lohász M, Rambaud P, Benocci C. LES simulation of ribbed square duct flow with FLUENT and comparison with PIV data. *CMFF'03*, *The 12th International Conference on Fluid Flow Technologies*, Budapest, Hungary, 2003.
4. Hoffman J, Johnson C. Computability and adaptivity in CFD. In *Encyclopedia of Computational Mechanics*, Stein E, De Borst R, Hughes TJR (eds). Wiley: New York, 2004.
5. Acharya S, Dutta S, Myrum TA, Baker RS. Turbulent flow past a surface-mounted two-dimensional rib. *Journal of Fluids Engineering* (ASME) 1994; **116**:238–246.
6. Hwang RR, Chow YC, Peng YF. Numerical study of turbulent flow over two-dimensional surface-mounted ribs in a channel. *International Journal for Numerical Methods in Fluids* 1999; **31**:767–785.
7. John V, Liakos A. Time-dependent flow across a step: The slip with friction boundary condition. *International Journal for Numerical Methods in Fluids* 2006; **50**:713–731.
8. Psychoudaki SP, Fragos VP, Malamataris NA. Computational study of a separating and reattaching flow. *IASME Transactions* 2005; **2**(7):1120–1131. ISSN: 1790–031X.
9. John V. Slip with friction and penetration with resistance boundary conditions for the Navier–Stokes equations—numerical tests and aspects of the implementation. *Journal of Computational and Applied Mathematics* 2002; **147**:287–300.
10. Oden JT, Prudhomme S. New approaches to error estimation and adaptivity for the Stokes and Oseen equations. *International Journal for Numerical Methods in Fluids* 1999; **31**:3–15.
11. Kraichnan RH. Inertial ranges in two dimensional turbulence. *Physics of Fluids* 1967; **10**:1417–1423.
12. Nazarenko S, Laval J-P. Non-local two-dimensional turbulence and Batchelor's regime for passive scalars. *Journal of Fluid Mechanics* 2000; **408**:301–321.
13. Batchelor GK. Computation of the energy spectrum in homogeneous two-dimensional turbulence. *Physics of Fluids* 1969; **12**:233–239 (ii).
14. Friedrich R, Huttl TJ, Manhart M, Wagner C. Direct numerical simulation of incompressible flows. *Computers and Fluids* 2001; **30**:555–579.
15. Moin P, Mahesh K. Direct numerical simulation: A tool in turbulence research. *Annual Review of Fluid Mechanics* 1998; **30**:539–578.
16. Hunt JCR, Sandham ND, Vassilicos JC, Launder BE, Monkewitz PA, Hewitt GF. Developments in turbulence research: A review based on the 1999 Programme of the Isaac Newton Institute, Cambridge. *Journal of Fluid Mechanics* 2001; **436**:353–391.

DOI: 10.1002/fld

17. Higdon JJL. Stokes flow in arbitrary two-dimensional domains: Shear flow over ridges and cavities. *Journal of Fluid Mechanics* 1985; **159**:195–226.
18. Gresho PM, Sani RL. *Incompressible Flow and The Finite Element Method*. Wiley: New York, U.S.A., 1998.
19. Ranacher R. Finite element methods for the Navier–Stokes equations. Preprint, Institute of Applied Mathematics, University of Heidelberg, 1999.
20. Le H, Moin P, Kim J. Direct numerical simulation of turbulent flow over a backward facing step. *Journal of Fluid Mechanics* 1997; **330**:349–374.
21. Colonius T. Artificial boundary conditions for compressible flow. *Annual Review of Fluid Mechanics* 2004; **36**:315–345.
22. Malamataris NA. Computer-aided analysis of flows on moving and unbounded domains: Phase-change fronts and liquid leveling. *Ph.D. Thesis*, University of Michigan, Ann Arbor, MI, U.S.A., 1991.
23. Malamataris NA, Panastasiou TC. Unsteady free surface flows on truncated domains. *Industrial and Engineering Chemical Research* 1991; **30**:2211–2219.
24. Papanastasiou TC, Malamataris N, Ellwood K. A new outflow boundary condition. *International Journal for Numerical Methods in Fluids* 1992; **14**:587–608.
25. Sani RL, Gresho PM. Résumé and remarks on the open boundary condition symposium. *International Journal for Numerical Methods in Fluids* 1994; **18**:983–1008.
26. Orlanski I. A simple boundary condition for unbounded hyperbolic flows. *Journal of Computational Physics* 1976; **21**:251.
27. Heinrich JC, Vionnet CA. On boundary conditions for unbounded flows. *Communications in Numerical Methods in Engineering* 1995; **11**:179–185.
28. Griffiths DF. The 'no boundary condition' outflow boundary condition. *International Journal for Numerical Methods in Fluids* 1997; **24**:393–411.
29. Renardy M. Imposing 'no' boundary condition at the outflow: Why does it work? *International Journal for Numerical Methods in Fluids* 1997; **24**:413–417.
30. Zienkiewicz OC, Taylor RL. *The Finite Element Method* (5th edn). Butterworth-Heinemann: Oxford, MA, U.S.A., 2000.
31. Kranjović S, Davidson L. Large Eddy simulation of the flow around a bluff body. *AIAA Journal* 2002; **40**:927–936.
32. Owen DRJ, Hinton E. *Finite Elements in Plasticity*: *Theory and Practice*. Pineridge Pr. Ltd.: Swansea, U.K., 1980.
33. Taneda S. Experimental investigation of the wakes behind cylinders and plates at low Reynolds numbers. *Journal of the Physical Society of Japan* 1956; **11**:302–307.
34. Malamataris NA, Bontozoglou V. Computer aided analysis of viscous film flow along an inclined wave film. *Journal of Computational Physics* 1999; **154**:372–392.
35. Malamataris NA, Vlachogiannis M, Bontozoglou V. Solitary waves on inclined films: Flow structure and binary interactions. *Physics of Fluids* 2002; **14**:1082–1094.
36. Schlichting H. *Grenzschicht-Theorie*. Braun: Karlsruhe, 1982.
37. Frisch U. *Turbulence*: *The Legacy of A. N. Kolmoforov*. Cambridge University Press: Cambridge, U.K., 1995.
38. Hinze JO. *Turbulence*. McGraw-Hill Book Company Inc.: New York, U.S.A., 1955.
39. Moon FC. *Chaotic and Fractal Dynamics*. Wiley: New York, 1992.
40. Sherman FS. *Viscous Flow*. McGraw-Hill Book Co.: New York, U.S.A., 1990.

DOI: 10.1002/fld